Simulated Syngas Ash Deposition on the Leading Edge of a Turbine Vane with Film Cooling

Eric Jeter Wood

Thesis submitted to the faculty of the Virginia Polytechnic Institute and State University
in partial fulfillment of the requirements for the degree of

Master of Science
in
Mechanical Engineering

Uri Vandsburger (Co-Chairman)
Wing F. Ng (Co-Chairman)
Danesh Tafti

August 11th, 2010
Blacksburg, VA

Keywords: Syngas, Deposition, Similarity

Simulated Syngas Ash Deposition on the Leading Edge of a Turbine Vane with Film Cooling

Eric Jeter Wood

Abstract

In using coal derived syngas in a gas turbine, solid particulates coming out of the gasifier can prove to be detrimental to the engine hardware. Not much is known about particle deposition, erosion, and corrosion on turbine blades as a result of these contaminants. Performing deposition studies at engine like conditions can be difficult due to the high temperatures of turbine engines. This study presents a method for substituting the particles with polymer materials so studies can be done under more workable conditions. PVC and Teflon particles were used and deposited against a flat plate to mimic a published experiment that used real coal ash. Temperatures were near the melting point of the material and oncoming momentum Stokes numbers were matched. It was found that using polymer materials is not a perfect substitute, but has the same trends and behaves in a similar fashion. All materials increase in deposition rate with free stream temperature and decrease in deposition rate as the surface is cooled.

PVC particles were then used in an experiment to impact a leading edge with film cooling. The same particle substitution method was used. It was found that increasing the free stream temperature increased the amount of deposition while increasing the blowing ratio slightly decreased deposition. Particle deposition on the leading edge tended to cause an increase in the film cooling effectiveness. It was also found that deposition on the surface slightly increased the convective heat transfer.

Acknowledgements

I would like to the U.S. Department of Energy and the University Turbine Student Research program for funding this study as well as my educational pursuits for the last two years. I also owe much thanks to my advisor, Dr. Uri Vandsburger, for giving me the opportunity to conduct research under his guidance and to attend graduate school. I am much appreciative of the other members of my committee, Dr. Wing F. Ng and Dr. Danesh Tafti, for their insight into this project. Colleague Sai Shrinivas has also been helpful in with his knowledge of the field.

I would not have been able to complete this research without Steve LePera, Chris Martin, and Joe Ranalli; all of whom have taken me under their wing and taught me how to work in the lab and conduct research. Also, thanks to all the undergrads and other lab associates who have assisted me with this research and heavy lifting.

Finally I would like to thank my mother and sister for supporting me over the years and all my friends and the Sigma Chi fraternity for making college fun.

Table of Contents

List of Figures

List of Tables

Nomenclature

Cool	Relating to coolant
CSDL	Combustion Systems Dynamics Laboratory
h	Convective heat transfer coefficient
MMD	Mass mean diameter
PLF	Particle loading factor
ppm	parts per million
PVC	Polyvinyl chloride
SCFM	Standard cubic feet per minute
SEM	Scanning electron microscope
St	Stanton number
Stk	Stokes number
Surf	Relating to the surface
T^*	Non-dimensional temperature
η	Film cooling effectiveness
∞	Relating to the free stream

1 Introduction

1.1 Background

Environmental, economic, and political issues have converged with the goal of developing cheap, reliable, and clean energy sources. One possible solution to this is coal gasification as part of an integrated gasification combined cycle (IGCC) plant. The essential part of this technology lies in the coal gasifier which converts solid coal into a synthetic natural gas, or syngas. Figure 1.1 is a schematic of how this type of gasifier operates, but other fuels such as biomass can also be used.

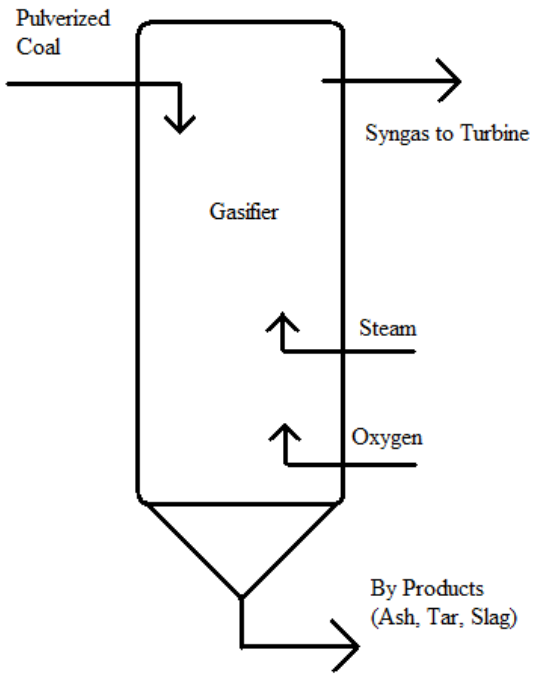

Figure 1.1. Schematic of typical coal gasifier

This process can be chemically described in Equation (1.1),

$$C_s + O_2 + H_2O \rightarrow H_2 + CO \quad (1.1)$$

Pulverized coal is solid carbon in that reaction. The resulting syngas is comprised of hydrogen and carbon monoxide, both of which can be burned in a gas turbine. However, this process also creates several by-products; one of which is ash. The ash can form particles in the gasifier and can be carried away by the syngas fuel stream. This fuel stream is hot, pressurized, and in large quantities, so filtering out the ash particles can be difficult. Current technology can filter out particles larger than 10μm, but smaller particles can get through and enter the turbine's combustor through the fuel lines. To complicate matters, filtration at the high gasifier temperatures can be difficult.

Over the course of one year of operation, a turbine using coal derived syngas could consume up to 2 tons of particulate matter [1]. As these particles in the hot gas path travel through the turbine section of the engine, there is potential for them to impact upon the blades and vanes. This may lead to deposition, erosion, and corrosion of the internal surfaces. If the particles block the coolant holes then total engine failure is a possibility since the air temperature leaving the combustor can be hot enough to melt turbine components. Degradation of the engine components could also lead to lower efficiency, lower power, and a lower lifespan turbine.

As particles pass through combustor they can breach their melting temperature and become molten. As a result, particles may make impact in both the solid and liquid phase. The exact composition of the syngas ash particles varies greatly, depending on where the coal comes from and how the gasifier is operated. Generally, the main constituents are silica (SiO_2), calcium oxide (CaO), aluminum oxide (Al_2O_3), and iron rust (Fe_2O_3), [2, 3]. This makes defining syngas ash difficult and can make particle properties, such as melting point, density, and size, vary from place to place.

1.2 Past Studies

Before coal derived syngas was to be used in land based gas turbines, this field of study examined particle ingestion in aircraft engines. Hamed [4] and Smialek et al. [5] studied sand particles that could enter aircraft engines during operation in the Persian Gulf. Hamed used 150μm sand and 15μm ash particles ingested in a helicopter engine. Hamed found that all parts of the blades were subject to impact, but the heavier sand

particles were more likely to impact than the lighter dust particles. Smialek used a wide variety of sand particles in military engines and found that sand particles under 10μm did not tend to impact on compressor blades before the combustor. However, when the sand particles become molten in the combustor, they did deposit on the turbine vanes. Plugging of cooling holes was observed and deposited coatings of up to 5mm were collected.

There have also been issues with jet engines flying through volcanic ash clouds. Kim et al. [6] studied the melting and deposition characteristics of volcanic ash from Mount St. Helens. Kim et al. found that the turbine inlet temperature and vane surface temperature were important factors in deposition phenomena. They also observed that the ash deposits that build up on the vanes can block cooling holes and cause damage. Figure 1.2 is a photograph of turbine vanes in a jet engine after volcanic ash has deposited from Kim et al. [6]. Note the plugged cooling holes and subsequent damage to the engine components.

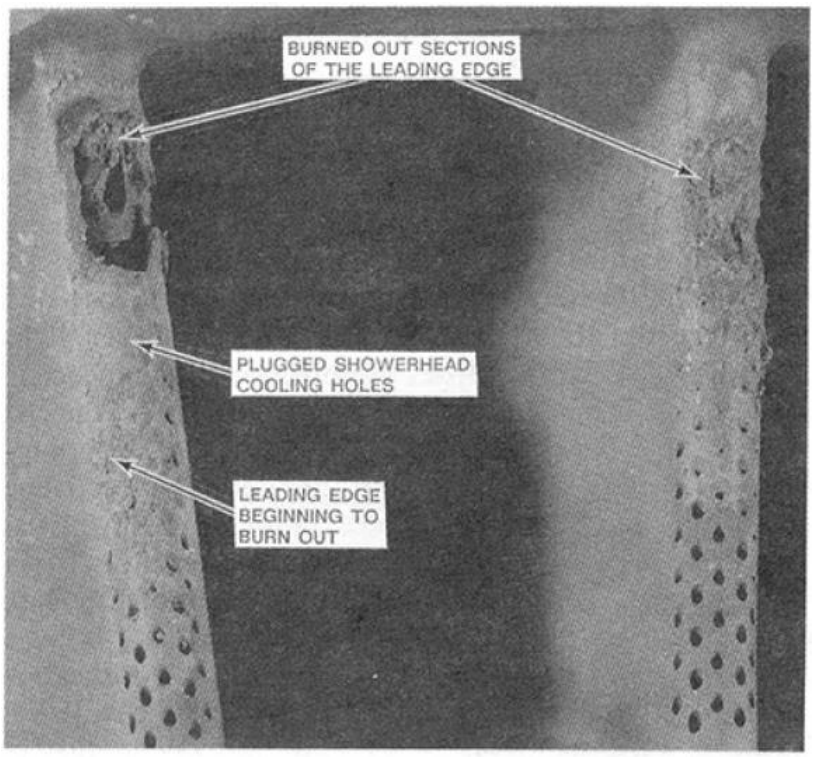

Figure 1.2. Photograph of vanes in jet engine with volcanic ash deposits. Note that the blocked cooling holes have caused damage. (From Kim et al. [6])

Hamed et al. [7] describe the causes of deposition to be: inertial impaction, turbulent diffusion/eddy impaction, Brownian motion, and thermophoresis. Larger particles have more momentum and deviate from the streamlines around the blades and can crash into the surfaces. Turbulent diffusion occurs when smaller particles become entrained in eddies near a surface and then their momentum can cause impaction on the surface. Brownian motion acts on very small particles (sub 0.1μm) in the flow by rapidly pushing the particles in random directions. This "random walk" can cause the particles to land on a surface and become deposited. Thermophoresis is a phenomenon that acts on particles immersed in a fluid with a temperature gradient. Gas molecules on the hotter side of the particle bounce off the particle more frequently than molecules on the cooler side. This resulting force causes the particles to drift towards to cooler direction. Since the surface of turbine vanes are cooled, particles are driven towards the surface and can potentially cause impaction.

Studies by Dring et al. [8] found good agreement between analytical and experimental results that particle trajectory and impaction are heavily dependent on particle size and velocity; which can be related to the particle momentum Stokes number. They also found that particles with a Stokes number below 0.1 generally follow streamlines around blades and Stokes numbers over 10 generally impact on the surface. Particles with a higher Stokes number tended to impact on the pressure side of the airfoil, via inertial impaction, while lower Stokes number particles were more likely to impact on the suction side via turbulent diffusion and thermophoresis.

The temperature of the free stream, and therefore the particle, also plays a major role in deposition physics. A particle that is closer to molten or actually molten is more likely to stick than their solid counterparts. Even if most of the particles are not in the molten phase, the few that are still contribute much of the buildup. Tabakoff et al. [10] found that particles that stick in their molten phase are less likely to detach and become re-entrained into the hot flow stream. Wenglarz and Wright [9] looked at land based turbines using synfuels and concluded that for particles whose delivery mechanism is dominated by inertial impaction, the particle's temperature in relation to its melting temperature is a strong predictor for deposition rates.

Another study by Wenglarz and Fox [11] have experimented with coal-water fuels (a type of slurry) in turbines and found that not only is deposition related to particle temperature, but also to surface temperature. Turbine blades are cooled to keep them under a safe operating condition and a cooler blade results in less particle deposition. Wenglarz and Fox found that the cooler the surface is, the less likely the particle is to deposit. This may be due to the particle cooling as it rears the colder surface and transitioning from the molten state to the solid state. Wenglarz and Wright also found that above a transition temperature deposition increases significantly. In their study, increasing gas temperature by 200°F increased deposition amounts by 2 orders of magnitude.

Other studies have confirmed the tendency for particles to stick more when the free stream temperature is increased and less when the surface temperature is decreased [12, 15, 14]. Logan et al. [12] and Ahluwalia et al. [13] reviewed several methods for lowering ash deposition in turbines. They both found targeted cooling surface to be an effective method for reducing unwanted ash buildup. Crosby et al. [14] used coal ash of various sizes at various free stream and surface temperatures. The trends shown were that smaller particles, cooler free stream, and cooler surface temperatures all favor less deposition. This particular study will be discussed at length later in Chapter 4.

Bons et al. [15] examined surface roughness patterns from many samples that came from actual turbine engines of four manufactures. Average surface roughness, root mean square roughness, peak to valley height, skewness, and kurtosis were measured. The study found that there was no single pattern to describe deposition shape, as spheres, cones, cliffs, and coating spallation were all found. Bons et al. also found that there was increased surface degradation around film cooling holes.

When turbine components become degraded from contaminants in the hot gas path, the engine can suffer. Wenglarz [15] studied a 50 MW coal-fired turbine at a firing temperature of 871 °C and how the concentration of particles in the hot gas path affected power. He found that when the turbine operates with 550 ppm (by weight) contaminants, the engine's output power can drop off 90% in just 20 hours. When the particle concentration is 58 ppm, 20% power is lost after 500 hours of operation. When the

engine is run at the lowest possible particle concentration, 0.01 ppm, the engine only lost 0.5% after 1000 hours of operation.

Bons has also studied the direct effects surface roughness has on heat transfer and skin friction inside turbines [17]. In this study, samples from in-service turbine hardware were subjected to deposit laden flow under various turbulence levels. It was found that the heat transfer (measured by Stanton number) was augmented by 10 – 50%. The skin friction coefficient was augmented by 30 – 300%. Another important find of this study was that simulated roughness (orderly pattern of cones or spheres) greatly under predicts these augmentations compared to real roughness. Higher turbulence levels also gave rise to higher Stanton number and higher skin friction coefficient. Increases of heat transfer and pressure drop (skin friction) away from the design point can be harmful to a turbine engine and lower its performance, as shown by Wenglarz [16]. The differences in simulated roughness and actual roughness observed in real engines are discussed at length by Bons et al. [15].

Another study by Bons et al. [18] looked into the augmentation of heat transfer on deposit laden surfaces in greater detail. This study simulated turbine conditions with a Mach number of 0.31 at a temperature of 1150 °C. The particle loading was such that it simulated one year of operation under a typical particle concentration of 0.02 ppm. The main finding in this report was that heat transfer was augmented each time more particles became deposited on the substrate, with a maximum augmentation of 30%. Bogard et al. [19] also studied the augmentation of heat transfer at conditions similar to a turbine airfoil. Here, heat transfer augmentations up to 50% were observed.

In addition to increases of heat transfer, there have been many reports of alterations to film cooling performance as surfaces become degraded [20, 21, and 24]. Schmidt et al. [20] used artificial surface conical elements whose height was 40% the diameter of the cooing holes. Surface locations 10 coolant hole diameters and more downstream saw a mild decrease (~10%) in cooling effectiveness for low blowing ratios, while seeing a small increase (~5%) for higher blowing ratios. Areas closer to the holes saw a mild increase (~10%) in film cooling effectiveness at higher blowing ratios and no significant change at lower blowing ratios.

Lewis et al. [21] and Ai et al. [24] both used samples from actual tests and not simulated roughness as recommended by Bons et al. [17]. These experiments were done on a flat plate angled 45° normal to the flow. The study by Lewis et al. found that there was actually less heat transfer and better cooling effectiveness downstream of the holes because of a "ramp up" effect. Deposits tended to form in the shape of miniature ramps immediately upstream of the cooling holes. This caused the hot air to deflect away from the surface and allowed the coolant to remain attached to the surface. It was also observed that some deposits formed in between coolant paths downstream of the holes. This "furrowing" effect also lowered heat transfer because deposits only formed where hot gas strikes the surface and the deposits caused an insulating effect in these areas. It was also noted that these deposition patterns around film cooling holes were also found on serviced hardware.

Ai et al. [24] confirmed these effects and also studied how hole spacing affected the film cooling. This study used a narrow and wide hole spacing at blowing ratios ranging from 0.5 to 4.0. The narrow hole spacing showed less deposition and had a better effectiveness. The major indicator for both configurations in terms of deposition amount was blowing ratio. There was a strong correlation of higher blowing ratio and lower capture efficiency. The effects to film cooling performance were similar to that of Lewis et al. [21].

Sundaram and Thole [22] conducted a scaled experiment to observe the effect of deposition on end wall film cooling. They found that film cooling could increase in effectiveness as a result of the deposited particles. This increase could sometimes be as much as 50% of the film cooling effectiveness value. However, this increase is limited because greater deposition heights would then decrease the film cooling effectiveness. They also found partial or complete blocking of the holes greatly diminished film cooling effectiveness. Lawson and Thole [23] measured the effect deposition had on a flat plate with film cooling with blowing ratios below 1.0. They found that deposition diminished film cooling effectiveness, but the reduction was not as great at higher blowing ratios. They reported a 20% effectiveness reduction at a blowing ratio of 0.23 and only a 6% reduction at a blowing ratio of 0.95.

Because of the findings of Wenglarz and Fox [11] and Wenglarz and Wright [9], it is known that the main mechanism of inertial impaction occurs at or near the melting or transitioning temperature of the particles. Coal syngas ash particles have a high melting point, around 1400 °C and depending on the constituents [25]. This means that experiments must be run at high temperatures that may be difficult to reach. To overcome this difficulty, it has been proposed that particles comprised of some other material may be used that have a lower melting point. This will allow the same deposition physics to be observed under more realistic experimental conditions.

A method for substituting the coal syngas ash particles for wax has been used by Lawson and Thole [23]. This experiment used air heated just to 42 °C and deposited the wax particles on a flat plate in line with the flow with film cooling. The size of the wax particles ranged from 1 - 200μm. The velocity in the experiment was adjusted to 8 m/s to give a Stokes number a range of 0.01 to 1000. This scaling method in comparison to engine conditions is discussed in greater detail later in Chapter 2. The conclusion from this study was that a momentum ratio of 0.95 was less susceptible to reductions in cooling effectiveness (6%) and lower momentum ratios (0.23 and 0.5) saw greater cooling effectiveness reductions (20%).

1.3 Objectives and Scope

The purpose of this study was twofold. First, a particle substitution method similar to Lawson and Thole [23] is presented. Instead of using wax particles, this method uses polymer particles made of Teflon and PVC. There are several advantages to this polymer substitution method over the wax method. Another part of the method discussed in this study is to scale the temperature of the free stream and surface with the melting point of the particles to produce scaling by non-dimensional temperature. This method is directly compared to syngas ash deposition experiments by Crosby et al. [14] for validation.

The next part of this study was to examine the role deposition has on the leading edge of a turbine component when there is film cooling present. All of the previous syngas ash experiments have been done on flat plates either in line with the flow or at a

45° angle thereof. This is important because the leading edge is the location where the hottest gas hits at stagnation and the most heat transfer occurs. The experiments in this part of the study used the particle substitution method outlined in the first part by using PVC as the particulate material.

The objective of this part of the study was to characterize how the deposits affect the performance. This was measured in part by net capture efficiency, a measurement of how many particles deposit on the surface. The changes in heat transfer (given non-dimensionally as Stanton number) and adiabatic film cooling performance before and after deposition has occurred will also be measured. The effect that varying the blowing ratio has these parameters will also be investigated. All deposition tests will be scaled in such a way to represent deposition build up after one year (8000 hours) of service at a typical particle concentration of 0.02 ppm by weight.

This study is being completed in alongside a CFD effort to predict deposits on the leading edge. Results from this study will be used to help validate the CFD method. A comparison of the experimental data found on the flat plate tests is reported by Sreedharan and Tafti [27]. Results from the experiments on the semi-cylindrical surface with film cooling will be compared to numerical results at some time in the future.

2 Particle Substitution Method

2.1 Material Substitution

In order to perform deposition experiments that match the real physics the temperature of the free stream needs to be comparable to the melting or transitioning temperature of the particles. Because syngas ash has a high melting point, ~1400 °C [25], experiments with these particles need to be run at or near temperatures found in the first stage of a turbine engine, ~1300 °C. It is difficult to sustain such high temperatures in an experimental setting, so a particle substitution method is proposed, similar to that of Lawson and Thole [23].

Instead of using wax, this method calls for some polymer product such as Teflon or PVC which is available in powder or particle form. The relevant properties of these materials are given in Table 2.1.

Table 2.1. Relevant material properties of Teflon and PVC

Material	**Teflon**	**PVC**
Melting Temperature (K)	600	533
Particle Diameter (μm)	8	24
Particle Density (kg/m^3)	2200	1390
Specific Heat (kJ /kg K)	1.17	0.9
Thermal Conductivity (W/m K)	0.25	0.16
Young's Modulus (Gpa)	0.5	3

In experiments that use particles, it is inevitable that not all particles are the same size. Therefore there is some ambiguity in the particle size used for calculations. The particle diameters reported in this study are based on the mass mean diameter. This is appropriate since it is of ultimate importance to consider the mass deposited and not the number of particles. To put it another way, the mass mean diameter (MMD) is the diameter of the particle that the average mass is in, instead of just the average particle size. The method for calculating the mass mean diameter is given in Equation (2.1):

$$d_p = \frac{\sum_i D_i^3}{\sum_i D_i^2} \tag{2.1}$$

For Teflon and PVC, the mass mean diameter was found by using an electron scanning microscope. Undeposited particles directly from the container were examined under the SEM and many individual diameters were measured. Using the formulae, the mass mean diameter was found and reported in Table 2.1. There was some variation in each; Teflon was between 3 – 10 μm and the PVC was between 10 - 35μm.

Teflon powder was obtained from DuPont, a product called Zoynl MP 1100. PVC particles have been obtained from Vinnolit Co., product number SA 1062/7. Both products come as a white powder and are readily available cheaply in large quantities. The chemical makeup of PVC and Teflon are drastically different from syngas ash because they are polymers. Even PVC and Teflon differ from each other being that PVC is classified as a vinyl polymer and Teflon is a fluorine based polymer.

These materials have a lower melting point than syngas ash so experiments can be conducted at lower temperatures. Non-dimensional temperatures are proposed for scaling in experimentation. This method also scales by the Stokes number to match the inertia of the oncoming particles, which is believed to be the driving mechanism for particle deposition. These scaling factors are outlined in detail below.

2.2 Scaling by Non-Dimensional Temperatures

Wenglarz and Wright [9] state that the particles temperature in relation to its melting temperature is important on predicting whether or not the particle will stick when inertial impaction is the primary force. Because of this, a non-dimensionalization of free stream temperature is given in Equation (2.2):

$$T_1^* = \frac{T_\infty}{T_{melt}} \tag{2.2}$$

T_∞ is the temperature of the free stream and T_{melt} is the melting temperature of the particle. If the particle being used has a lower melting point, this allows the experiment to be conducted at a lower temperature while matching the non-dimensional temperature in an actual engine.

Wenglarz and Fox [11] show that the surface temperature of the deposition substrate also plays a pivotal role in deposition physics. For this reason, a second non-dimensional temperature is proposed. Equation (2.3) is another non-dimensional temperature that takes the surface temperature into account as well

$$T_2^* = \frac{T_{melt} - T_\infty}{T_{melt} - T_{surf}} \tag{2.3}$$

In this equation T_{surf} is the temperature of the surface on which the particles are deposited. This non-dimensional temperature was picked such that its value ranges from 0 – 1; one meaning that there is no cooling and the surface temperature matches the free stream. All numbers below 1 indicate cooling and the lower T_2^* indicates more cooling. It is important to note that when varying T_2^* in an experiment, it is assumed that the free stream is held constant and only the surface temperature is varied. This will allow for a direct measure of how surface temperature affects deposition characteristics.

2.3 Scaling by Stokes Number

Because particle inertia is the driving factor for deposition in these studies, the momentum of the oncoming particles needs to be considered. Dring et al. [8] showed that the Stokes number is good indicator of wheter or not a particle in the hot flow will impact upon the surface. The Stokes particle momentum number is a ratio of a viscous time scale of a particle in flow to a stopping time scale of some target. This Stokes number has been defined in Equation (2.4):

$$Stk_p = \frac{\tau_v}{D/u_\infty} = \frac{\rho_p d_p^2/18\mu}{D/u_\infty} \tag{2.4}$$

In this equation, ρ_p is the density of the particle, d_p is the mass mean diameter of the particles (defined in Equation (2.1)), μ is the viscosity of the fluid, D is the diameter of the target (in this case the leading edge), and u_∞ is the free stream velocity. This particle substitution method calls for matching the Stokes number as well. This is done through a trade-off of particle size and particle velocity. Since Teflon and PVC have larger particles, their velocity during experimentation should be less.

As stated, this is similar to the method employed by Lawson and Thole [23], but is more realistic to actual turbine flows. From their paper, it is estimated that the mass mean diameter for the wax particles to be 100μm. A comparison of flow conditions between syngas ash in an engine, the Lawson and Thole wax method, and this polymer method is given in Table 2.2. Real engine conditions were assumed to be typical. The polymer material used for calculations is PVC and the leading edge diameter is assumed to be 0.025m.

Table 2.2. Comparison of particle substitution methods to real engine conditions

	Real Engine	**Wax Substitution [23]**	**PVC Substitution**
$\mathbf{T_1^*}$	0.95	0.95	0.95
$\mathbf{T_{melt}}$ **(K)**	1673	329	533
$\mathbf{T_\infty}$ **(K)**	1590	314	505
$\mathbf{U_\infty}$**(m/s)**	400	8	30
$\mathbf{d_p}$ **(μm)**	5	100	24
Stokes number	0.8	9	3
Reynolds number	39,000	13,000	26,000
Mach number	0.5	0.022	0.067

For the PVC substitution method, the Stokes number, Reynolds number and Mach number are all closer to the real engine conditions compared to the wax substitution method. For this reason, it was determined that the PVC substitution method presented in this study will provide more accurate results.

2.4 Particle Loading Factor and Capture Efficiency

Another aspect of this scaling method has to do with the particulate loading. Real engines don't see substantial build up that affects performance until after about 1 year of operation. Wenglarz [16] showed that engines at very high particulate loading (550 ppm) saw a substantial drop off in power after only a few hours. Lower particle concentrations (0.01 ppm) could operate for over 1000 hours without seeing any substantial decrease in engine performance.

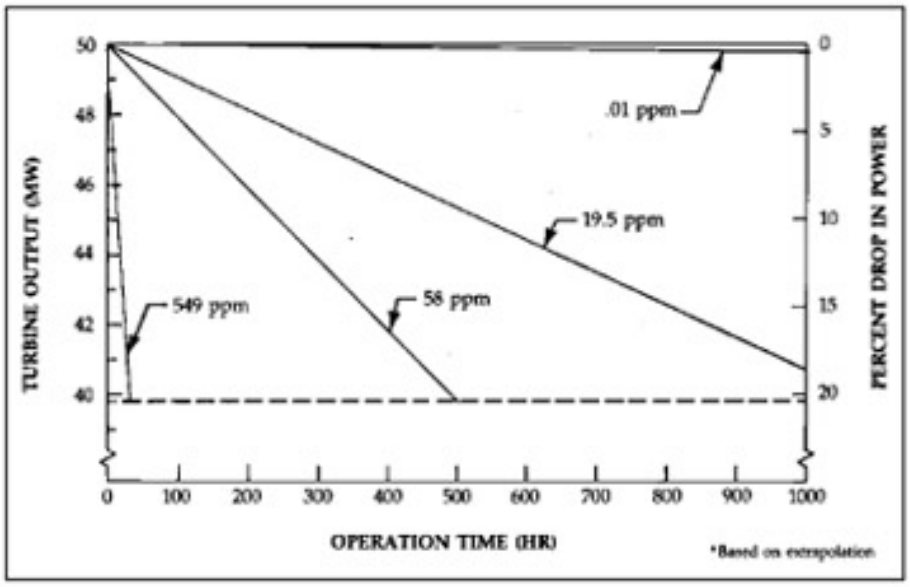

Figure 2.1. Reductions in power for several particle concentrations [16]

Typical engines that coal derived syngas typically have a particle concentration on the order of 0.02 ppm (by weight), as reported by Jensen et al. [26]. From the data Wenglarz obtained with the 50 MW turbine, it is predicted that an engine running with a particle concentration of 0.02 ppm would see a 5% drop off in power after approximately 10,000 hours of operation.

In order to conduct experiments in a reasonable timeframe, Jensen et al. [26] propose a tradeoff between particle concentration and exposure time. This would mean that the particle concentration is greatly increased and the exposure time is greatly decreased. A particle loading factor (PLF) is proposed in Equation (2.5).

$$PLF = \left[\frac{Mass\ flux\ of\ particles}{Mass\ flux\ of\ air}\right] * \ time \tag{2.5}$$

The units for the PLF are in ppmw-hr. A real engine that has a particle concentration of 0.02 ppm and runs for 10,000 hours will have a total PLF of 200 ppm-hr. In the study by Jensen et al. [26], a particle concentration of 50 ppm was used and the test was run for about 4 hours. This yields the same PLF as the real engine that they were simulating.

The lines shown in Figure 2.1are all straight linear lines with the same vertical intercept, they just differ by slope. If the slope of those lines were divided by their particle concentration, the lines would come close to converging. This transform is essentially what the PLF does. Another way to put this is that the time associated with power degradation (slope of the lines) times the respective particle concentration (ppm) should be a constant for all the cases.

The same method is proposed for this study. Particle concentrations for this study will be even higher than in the study by Jensen et al. Teflon and PVC concentrations will be on the order of 1000 ppm (by weight) and tests will be completed after about 10 minutes of deposition.

The amount of particles that deposit on the surface is an important parameter to acquire. Because of differences in the particle loading, a straight comparison of experiments to actual hardware in terms of g/mm^2 or number of particles per area is insufficient. A non-dimensional term called capture efficiency has been used in the literature [14, 18, and 26]. Although exact definitions can vary depending on the experiment, for this study, the capture efficiency is defined in Equation (2.6):

$$\epsilon = \frac{\mathrm{m_{deposit}}}{\mathrm{m_{approach}}} \tag{2.6}$$

The capture efficiency is the ratio of the mass of particles deposited on the surface to the mass of particles that approached the surface over the course of the run. For

example, 100 1 mg particles are evenly dispersed in a flow field approaching a surface. The ratio of the area of the surface normal to the flow to the cross sectional area is ¼. This means that only 25% of the particles (25 particles in all) in the flow will approach the surface while the other 75% do not have a chance of deposition. After the experiment, it is observed that 5 of the 1 mg particles have deposited on the surface. Using this definition, the capture efficiency would 5/25, or 20%. The capture efficiency would not be 5% (5/100) as others might have defined the term.

Definitions of capture efficiency differ because others have used the mass of all particles injected during the experiment in the denominator while some had an area ratio of 1:1. This means that the cross sectional area of the flow field and the normal to the flow area of the coupon are the same. It is not that one way of defining the term is better than another, but it is good to clarify.

3 Experimental Methodology

3.1 Facility Overview

All experiments presented in this study have been executed at the Combustion Systems Dynamics Laboratory (CSDL) at Virginia Tech. The central line is the Modular Combustor Rig and can have its sections replaced as needed for whichever experiment is needed. Figure 3.1 is a photograph of the main line setup for to run deposition experiments on a flat plate, which will be discussed in Chapter 4.

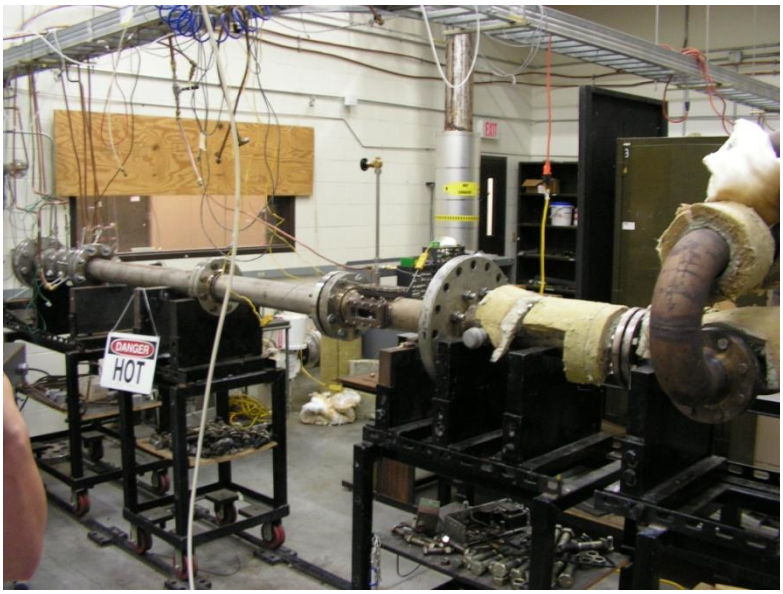

Figure 3.1. Photograph of CDSL's main line that is setup for the flat plate deposition experiment

Coming into the main line is air from a large air compressor made by Kaeser Compressors. Air flow rates can be supplied up to 1250 SCFM and at pressures up to 10atm. Between the compressor and the main line is a large electric air heater made by HEAT Inc. This heater has a maximum thermal output of 300kW and can heat air up to approximately 1000 °F. The exhaust air is sent up a stack so particle laden air is not reused. All test sections are made from stainless steel so they can withstand high temperatures and elevated pressures.

The experimental conditions are setup and controlled in the control room. The heater is controlled by a Watlow controller using a PID system. Valves controlling the pressure and flow rates are controlled and monitored by a LabView program. This LabView program can read in signals from pressure transducers, valve settings, thermocouples, and mass flow meters to arrange the proper experimental conditions.

3.2 Measuring the Deposition Amount

In order to find the capture efficiency for each case, the mass of particles deposited on the surface needs to be measured. Two methods for doing this are presented. One way uses a surface profiler to make many scans and derive the mass deposited from the surface roughness. The second method directly weighs the mass of the particles that have deposited on the surface.

Using a contact surface profiler to determine the deposition amount has previously been used successively by Jensen et al. [26]. The surface profiler used for this measurement was a computerized device named the Alpha Step 500, made by Tencor. The device made 2.5mm scans with a vertical resolution of 1μm. The deposition surfaces were polished prior to being used in the experiment to eliminate natural roughness. This ensured that all measured roughness was from the particles and not deformities in the metal surface. For each of the samples, which were 2.54 cm in diameter, 20 individual scans were made all over the surface. Figure 3.2 is a photograph of a sample with lines drawn in showing typical location of the 20 scans. The scans were made at random locations around the sample to get the best representation of the surface roughness for the entire sample.

Figure 3.2. Typical location of surface scans for measuring deposition

Each scan was 2.5mm in length, for a total scanning length of 50mm. Every scan was integrated and divided by its scan length to give the average roughness for that area. Figure 3.3 is a sample surface scan when PVC was deposited on a flat plate. The 20 roughness measurements were then averaged for a total roughness measurement for the whole surface. This total average roughness was then be integrated across the whole coupon surface to get the average volume of roughness. Since it is assumed that all of the roughness measured is from deposited particles, an approximation of the amount of particles deposited can be obtained. This method is equivalent to finding the volume by double integrating the thickness multiplied by the density of the particles as given in Equation (3.1):

$$m_{dep} = \rho_p \iint t \, dA \tag{3.1}$$

Where m_{dep} is the approximate mass deposited, ρ_p is the particle density, and t is the measured thickness.

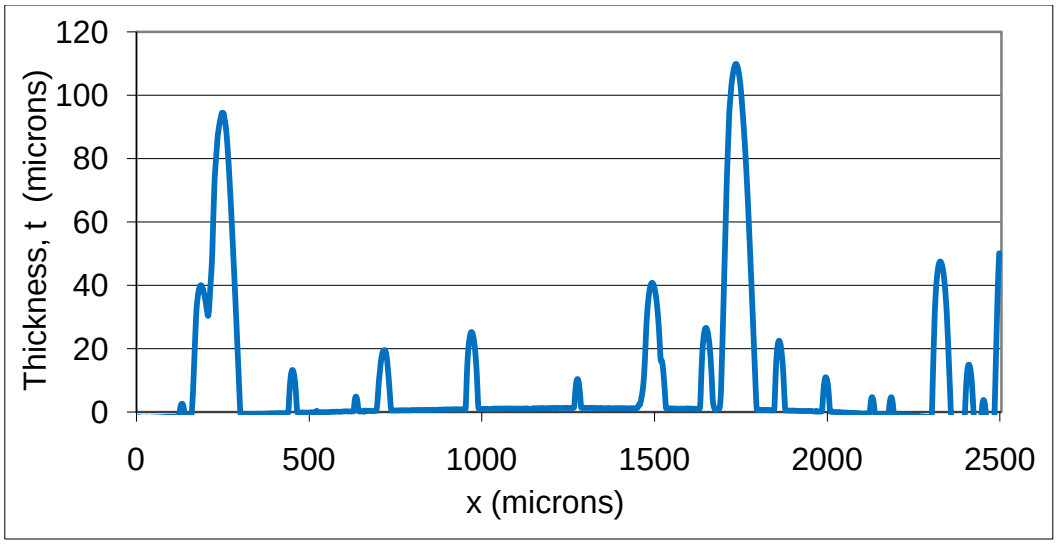

Figure 3.3. Sample surface scan for measuring deposition (PVC)

There are a few concerns associated with this method. The first is that the surface is rough from machining and this would be measuring that roughness instead of the particles. This concern was taken care of by polishing the surfaces until they were shiny prior to conducting the experiment. A polished blank sample was scanned under the profiler machine and the roughness was found to be less than 1μm (the resolution limit of the equipment). Since the particles were on the scale of about 20μm, the signal to noise ratio was considered to be suitable. This is confirmed by examining Figure 3.3; the 'zero' thickness layer corresponds to the sample's surface. The bottom layer can be seen to be smooth compared to the large bumps which represent the particles. The other concern is that the contact profiler pushes some of the particles out of the way, almost like a snow plow. The Alpha Step 500 has a small mounted camera that watches the contact point as the scan happens. Instances of the profiler moving particles were very rarely seen (only twice). Almost every time the contact would successfully measure the particles. Also, the contact stylus point only has a force of 10μN, so the surface was profiled delicately.

The other method used for finding the mass deposited on the surface was to use a very sensitive scale and directly measure the weight of the particles. A professional mini scale made by High Weight (model number SCL-D20) was obtained for these measurements. This small digital scale has a resolution of 2mg, and can measure masses

up to 20g. Crosby et al. [14] used a similar method of direct mass measurement for their experiments with success.

After an experiment was completed, the surface was scraped off using some plastic fishing line. For the surfaces with cooling holes, a small wire was used to push all the deposits out and ensure that all particles are removed. The particles were stored in small plastic bags until it was time to measure the mass. Each empty plastic bag weighed 1.030g with little variation. This mass was subtracted from the mass measured with particles such that only the mass of the particles is counted. For example, after the particles have been scraped into the bag, the whole bag is measured. If the scale reads 1.342g, then the total mass of the particles on the surface would be 0.312g (1.342 – 1.030 = 0.312g). A photograph of the scale with a baggie of deposits is shown in Figure 3.4.

Figure 3.4. Photograph of scale used to measure mass of deposited particles

3.3 Surface Temperature Measurements

The process for measuring surface temperature and its related parameters is central to this study. For both experiments on the flat plate and the semi-cylindrical surface, the surface temperature needs to be known in order to specify T_2^* in Equation (2.3). For the experiments on the semi-cylindrical surface with film cooling, the surface temperature is also needed to find the film cooling effectiveness (η) and the convective heat transfer coefficient (h).

The flat plate experiment will be discussed in detail later in Chapter 4 (see Figure 4.2), but the surface was cooled by a coolant system completely separate from the main hot air flow. This is unlike the film cooling case because the coolant jets mix with the free stream. The surface temperature of the flat plate was controlled by changing the coolant flow rate via a valve. For calibration purposes, a thermocouple was attached directly to the surface which was later removed as to not interfere with the deposition process. There was also a thermocouple attached to the backside of the plate where the coolant is impinged. It can be said for this geometry that the surface temperature is a function of only the free stream air temperature, the free stream velocity, and the temperature of the backside. These three parameters determine the convective and conductive heat loads that have to be in balance and set the surface temperature. Therefore, if two of those three parameters are held constant, it can be said that the surface temperature is only a function the third. With this in mind, the system was characterized by calibrating the surface temperature to the backside temperature while holding the free stream velocity and temperature constant. This was done so that when the deposition tests are underway, the surface temperature can be determined without having a direct reading (i.e. a thermocouple attached). For this kind of calibration, the free stream velocity was held constant at 2.6 m/s and the free stream temperature was held constant at 173°C. Then the coolant flow rate was varied and the backside vs. surface temperature correlation was characterized. This calibration curve is shown in Figure 3.5

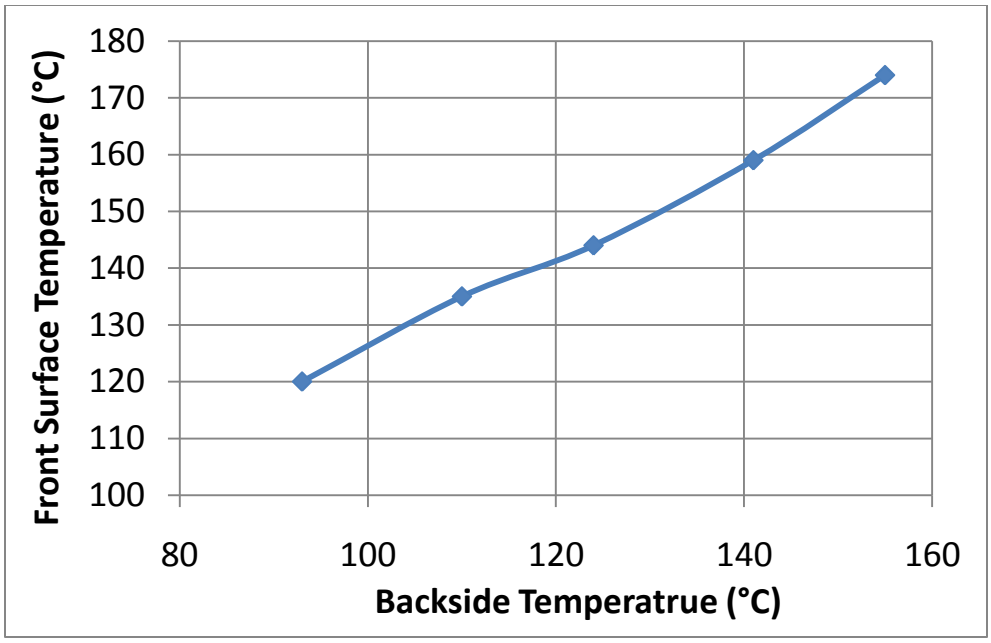

Figure 3.5. Calibration curve for surface temperature for flat plate experiment

Using this graph, the front surface temperature can be known without any direct obtrusive measurement. For example, if during the experiment it is desired to have the front surface be 140°C while the free stream is at 173°C and 2.6 m/s then this calibration curve is used. The coolant flow rate is adjusted until the thermocouple on the backside reads 120°C. Then once everything reaches steady state the particle deposition can begin. A separate calibration curve was created for the Teflon experiments because those were done at a free stream temperature of 191°C and velocity of 4.6 m/s.

The surface temperature measurement for the case with the semi-cylindrical surface is more involved than just determining one number. A thermocouple was not used for these measurements, but an infrared radiation (IR) camera that can map out surface temperature unobtrusively from a distance. The IR camera used here was made by FLIR and is model # SC640. For this set of experiments, T_2^* (Equation (2.3) is not an independent variable, but rather a dependent variable that is a function of the blowing ratio. The IR camera can record the average surface temperature at each blowing ratio and then calculate T_2^*, which will be reported.

IR cameras work by spatially resolving the amount of infrared radiation emitted from a surface. Infrared radiation covers the electromagnetic spectrum range from about 0.7 to 300μm, which have longer wavelengths than visible light (below 0.7μm). As a surface

becomes hotter than its surroundings, it will emit thermal radiation. The hotter the surface is, the more radiation it emits. This radiation can be detected with the IR camera and resolved into a temperature. The total power a surface emits has been defined by the Stefan-Boltzmann law, shown in Equation (3.2):

$$\mathrm{P} = A\varepsilon\sigma T_{surf}^{4} \tag{3.2}$$

Where A is the area of the surface, T_{surf} is the surface temp (assuming the surroundings are at absolute zero), σ is the Stefan-Boltzmann constant, and ε is the emissivity. A true black body has an emissivity of 1, but objects that emit thermal radiation are not true black bodies. Therefore, the emissivity of the surface needs to be known in order to get an accurate temperature reading.

In order to get the semi-cylindrical surface as close to a black body as possible, the surface and the inside of the test section was all painted black with high temperature resistant paint. Then the IR system was calibrated to find the actual emissivity. This was done by attaching a thermocouple to the surface and heating the incoming airflow to test conditions. The emissivity is found by comparing the hard thermocouple temperature reading to the IR camera's reading at the same point. The emissivity for the black painted surface and through the IR window was found to be 0.975.

This temperature measurement using IR is also used when deposits have formed on the surface. This could present an additional problem because the particles may not have the same emissivity as the bare black metal. There is no simple way to resolve this difference in the IR data reduction because the IR camera does not know which pixel is bare black metal and which pixel is particulate matter. To predict the error from this discrepency, the emissivity of some materials was directly measured. PVC, paraffin wax [23] silica (largest constituent of coal ash), and black painted metal were all soaked in an ice bath so that their temperatures were known to be 0°C. Then, through the IR window, their infrared radiance was measured with the IR camera and their emissivity was found. Although emissivity can change with temperature, effects are thought to be small for the experimental range. The emissivity for these materials at 0°C is given in Table 3.1.

Table 3.1. Emissivity of various particulate materials at 0°C

Material	**Emissivity, ε**
Bare Black Metal	0.98
Glass (silica)	0.90
Paraffin wax	0.96
PVC	0.93

To put this in terms for this experiment, if the IR camera is looking at a surface of PVC and thinks it is bare black metal, then the temperature reading will be 1.3% lower. Although it is desired to avoid all errors in this measurement, an error this small is acceptable when measuring the temperature of a PVC particle laden surface. It should be noted that the error is greater when using silica or coal ash particles, as others have done in experiments.

Due to the geometry and setup of the semi-cylindrical surface with a flat after body experiment (Figure 5.9), it was difficult to get a clear image of the entire leading edge. Because a 2-D image is taken of a curved surface, each pixel does not represent the same amount of area. This creates a problem when the area-averaged surface temperature is desired. The setup also presents a difficulty in determining which row of pixels corresponds to what degree from stagnation. To further complicate matters, the IR camera was placed at a viewing angle to get the best possible shot if the leading edge. To better illustrate these issues, Figure 3.6 shows a schematic of the semi-cylindrical surface in the hot gas path. Note that the IR camera is outside of the sealed test section and views the surface through an IR window.

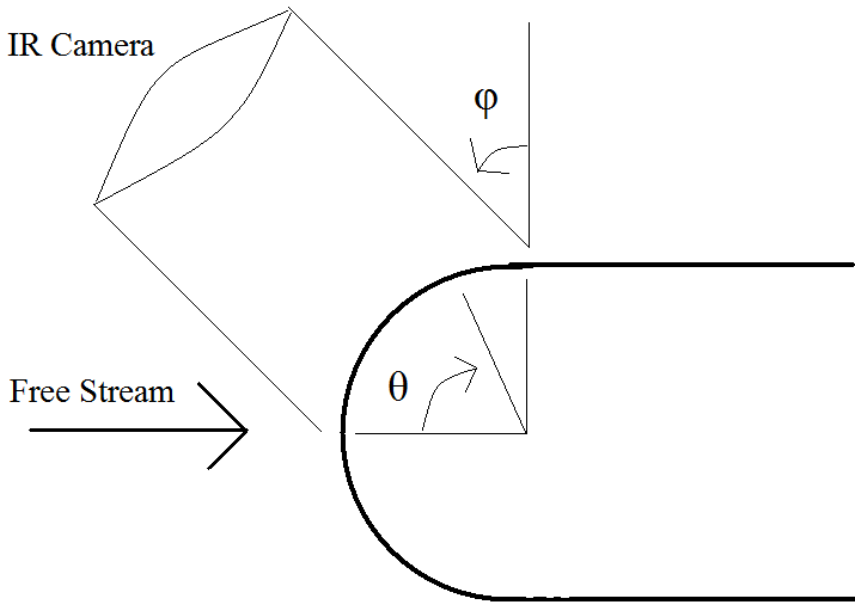

Figure 3.6. Schematic of the IR camera angle in relation to the semi-cylindrical surface

The IR camera is placed at a viewing angle from the vertical, φ, and the degrees from stagnation are represented by θ. For this experiment, the viewing angle φ was 20°. Surface temperature and effectiveness will be presented as functions of degree from stagnation, θ, which ranges from 0 - 90°. These difficulties were resolved through post-processing of the data after the images were taken. The Matlab program used to perform this geometric transform is available in the appendix.

The area-averaged temperature is resolved by applying a weight factor to each angle from stagnation (or row of pixels). A pixel observed near stagnation is viewed at an extreme angle such that it represents more area of the surface than a pixel at 45°. Therefore, the pixels near stagnation get more of a weight than the pixel at 45°. This relation is demonstrated in Figure 3.7, which plots the given weight factor for each angle from stagnation. Note that at 70° the weight factor equals 1. The reason is that this angle directly lines up with the viewing angle of the IR camera (90 – 20 = 70°).

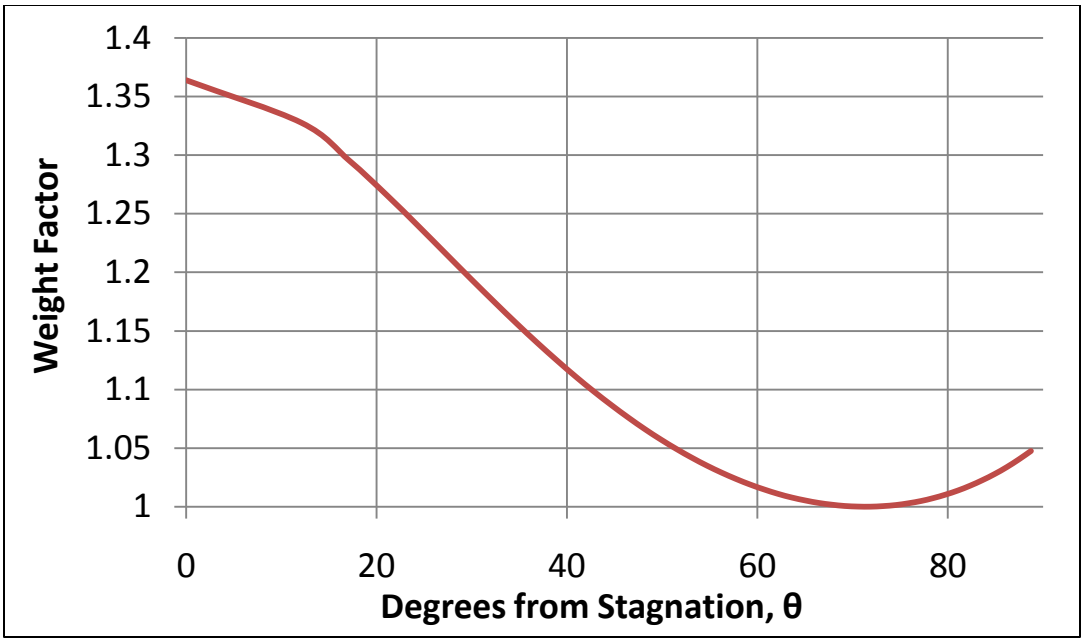

Figure 3.7. Weight Factor vs angle for spatially resolved temperature

Using the weight factor method, the area-averaged surface temperature can be calculated. This allows for the determination of T_2^* in Equation (2.3), as well as the adiabatic film cooling effectiveness.

3.4 Film Cooling and Heat Transfer Measurements

The adiabatic film cooling effectiveness is a widely used term to evaluate how well a surface is cooled and is defined in Equation (3.3) as:

$$\eta = \frac{T_\infty - T_{aw}}{T_\infty - T_c} \tag{3.3}$$

T_∞ is the free stream air temperature, T_c is the coolant temperature, and T_{aw} is the adiabatic wall temperature. Since T_∞ is the hottest temperature, and T_c is the coolest temperature in play, T_{aw} will be somewhere in between and η will be between 0 and 1. If it is 0, then the surface is the same temperature as the free stream. Subsequently, if η is equal to 1, then the surface temperature is the same as the coolant temperature. This can

be calculated locally where the adiabatic wall temperature is found at a single point, or globally where the temperature is averaged across the whole area.

The adiabatic wall temperature is directly related to the surface temperature. Adiabatic means without heat transfer, so the adiabatic wall temperature is the surface temperature when there is no heat conduction through the surface. This can be found by two methods. The first is to use a material that has high thermal insulating properties / low thermal conductivity. Any material made from a plastic would have sufficiently low thermal conductivity such that the surface temperature would be equal to the adiabatic wall temperature.

However, it may be desired to conduct experiments at high temperatures that would melt or greatly weaken plastic materials. In this case, a method for determining the adiabatic wall temperature from the surface temperature has been devised. Derived from the conservation of energy and similar to a method used by Cutbirth [28], the amount of heat lost into the surface can be back calculated. See Figure 5.8 for clarification. The conduction into the surface can be estimated and an approximate adiabatic wall temperature can be found:

$$T_{aw} = T_{meas} + \Delta T_{cond} \tag{3.4}$$

Where T_{meas} is the measured surface temperature at any given location and ΔT_{cond} is the amount of temperature drop the surface experiences due to conduction into the coolant plenum. The main assumption here is that the blade experiences constant surface heat flux from the hot mainstream flow into the coolant plenum. Because the blade's walls are of uniform thickness, the surface temperature drop can be found by:

$$\Delta T_{cond} = \dot{m}_c c_p (T_c - T_0) \frac{l}{k_{ss} A} \tag{3.5}$$

Where m_c is mass flow rate of the, c_p is the specific heat of the coolant air, T_c is coolant jet temperature as it exits the blade's plenum, T_0 is 0°C (cooling air enters at from ice bath), L is blade wall thickness, k_{ss} is the thermal conductivity of the surface material

(stainless steel), and A is the surface area of the whole blade. ΔT_{cond} will always be positive because the coolant air will heat up as it travels through the plenum and exits through the cooling holes. The assumption of constant surface heat flux is not ideal, but should suffice for this experiment in order to get the adiabatic cooling effectiveness.

Besides the film cooling effectiveness, it is also of interest to find the convective heat transfer coefficient. While the cooling effectiveness is found under steady-state conditions, the convective heat transfer coefficient, h, is found under transient conditions. This method uses a 1-D lumped capacitance approximation with a low Biot number. For this experiment, the Biot number was below 0.1 and considered sufficient. However, if the material of the surface is plastic, then the Biot number become greater than one and this method cannot be used. When the blade undergoes a sudden change of heat transfer conditions (i.e. free stream velocity or temperature), the surface temperature will change with time until it reaches some new steady equilibrium state. During this transition, the surface temperature can be recorded as a function of time and the heat transfer coefficient, h, can be deduced as an exponential relation described by Abuaf et al. [29].

$$\frac{T_{ss} - T_{surf}(t)}{T_{ss} - T_i} = e^{(\frac{-h}{\rho l c_p})t} \tag{3.6}$$

Rearranging Equation (3.6) to solve for h yields:

$$h = -\ln(\frac{T_{ss} - T_{surf}(t)}{T_{ss} - T_i})\frac{\rho l c_p}{t} \tag{3.7}$$

Where T_{ss} is the steady state temperature, T_{surf} is the measured surface temperature, T_i is the initial temperature (at time equal to zero), ρ is the density of the stainless steel, l is the wall thickness, and c_p is the specific heat of the material. The h value can be measured at several times during a single test and all should give the same value. For accuracy, the reported h value will be the average of a few hundred separate measurements throughout the test.

For this experiment, the sudden change to the heat transfer conditions required a step change to the free stream air temperature. When the thermal and fluid conditions reached steady state (30 m/s and 485K), a spray nozzle upstream of the blade was turned on. The water spray cooled down the air temperature hitting the surface through evaporative cooling. After a few minutes of this, a new steady state had been reached where the surface is cooler than it originally was. At this point, the water spray is quickly closed so no more evaporative cooling was taking place. The free stream air temperature experiences a step change, which subsequently affects the heat transfer into the body. Figure 3.8 is a graph of the free stream temperature experiencing this step change when water spray was turned off.

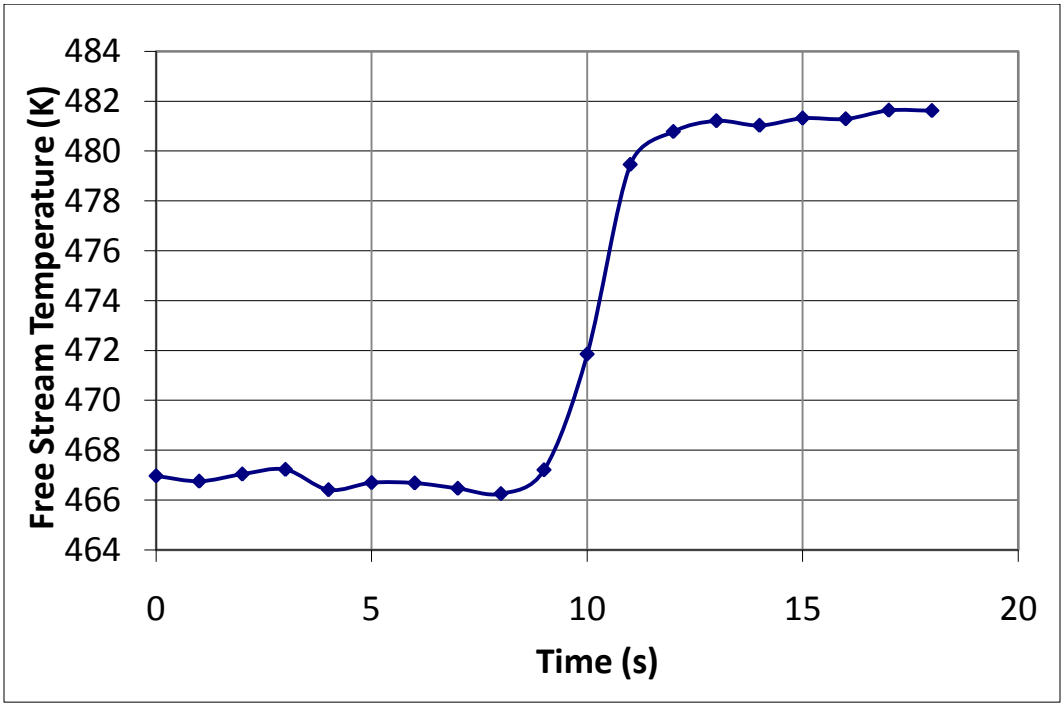

Figure 3.8. Step change in free stream air temperature for transient analysis

The leading edge of the blade body reacts to this step change in free stream temperature by heating up to its new steady state. The quicker the surface heats up, the greater the convective heat transfer coefficient is. The transient surface temperature was measured at three points along the leading edge; at 20°, 40°, and 60°. A sample graph of the transient surface temperature measurement is given in Figure 3.9.

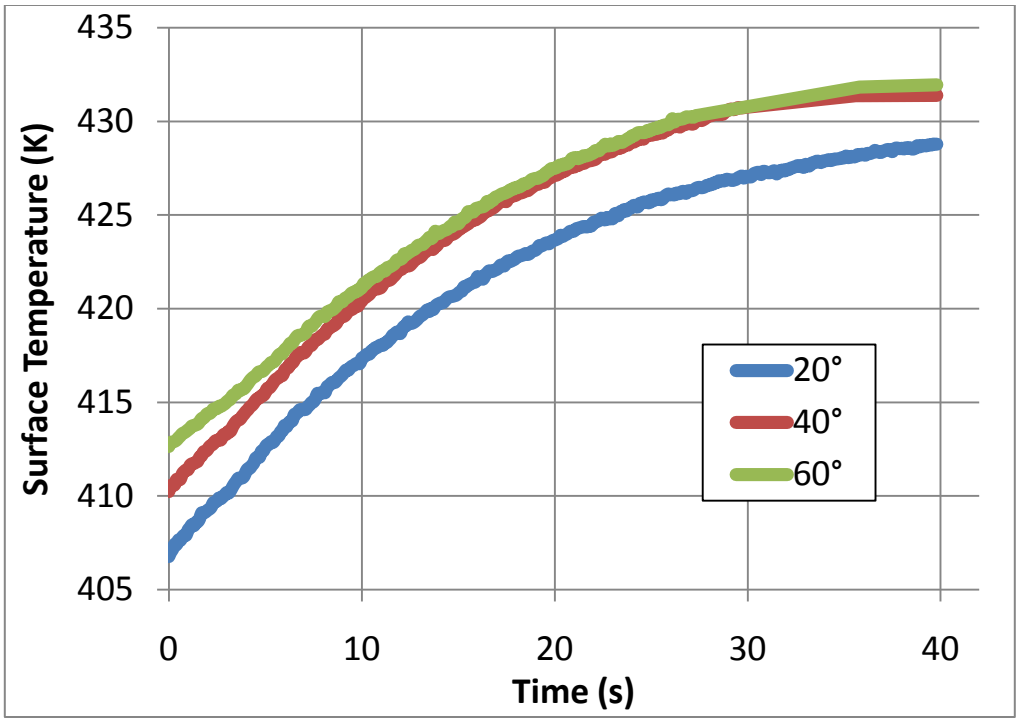

Figure 3.9. Sample graph of the transient heat transfer measurement

The shape of the exponential curves in Figure 3.9 is what determines the heat transfer coefficient. The curves are put into Equation (3.7) and a value of h can be found for each point. Data was collected at 10 Hz, so 40 seconds of data yields 400 data points. A unique value of h can be found at each of these data points (or one per 0.1 sec). Reported values are the averaged value for all data points.

Further, the convective heat transfer values will be reported as a non-dimensional number by the Stanton number. The Stanton number is defined as:

$$St = \frac{h}{c_p \rho U} \tag{3.8}$$

Where c_p is the specific heat of the fluid, ρ is the density of the fluid, and U is the free stream velocity of the fluid.

4 Experiments on a Flat Plate

4.1 Review of Crosby's Experiment

Experiments have previously been completed by Crosby et al [14] at Brigham Young University at the Turbine Accelerated Deposition Facility. These experiments used real coal ash particles heated to engine-like conditions and traveling at engine-like velocities. The goal of the study was to characterize the independent effects of particle size, gas temperature, and metal temperature on deposition. The experiment consisted of a 1" tube ejecting hot particle laden flow that impinged onto a 1" angled flat plate that could be cooled. The coolant system is completely separate from the hot gas and there are no film cooling or cooling holes. Figure 4.1 shows this setup.

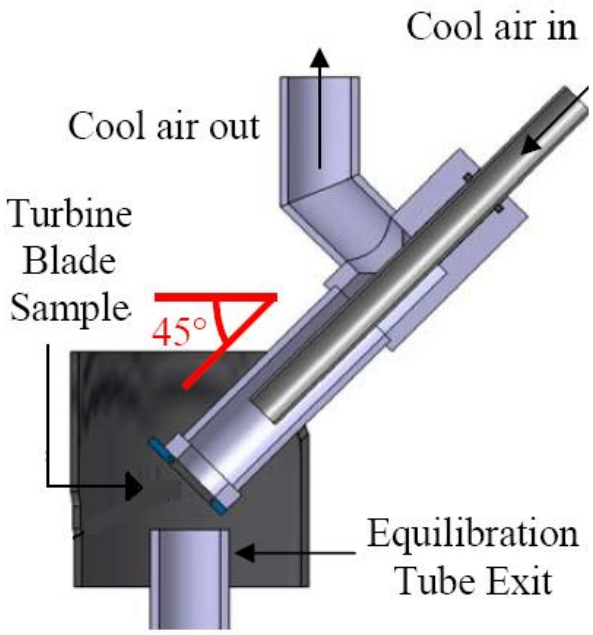

Figure 4.1. Setup of deposition experiments at BYU [14]

Crosby's experiment included particles is the range of 3 - 16μm composed of either petcoke or coal ash particles. The flow was heated to around 1200°C at an exit velocity of 170 m/s. These fluid and thermal conditions are similar to those seen in real turbine engines. This is what allows this experiment to use real coal ash as the particulate material instead of a substitution material.

For the case with varying the particle size, it was found that increasing the particle diameter tended to increase the capture efficiency (relative mass deposited, Equation (2.6) while holding everything else constant. This is expected because other experiments have shown that that increasing the particle momentum Stokes number (Equation (2.4) also increases the capture efficiency and the Stokes number is heavily dependent on particle diameter.

The other main conclusions from this study were that increasing the hot gas temperature also caused the capture efficiency to increase. This relation is exponential with hardly any deposition seen at temperatures below 900°C and higher capture efficiency (~2%) seen at 1200°C. The exponential relation here implies that decreasing the free stream small amount can pay off with a large decrease in capture efficiency. A series of experiments was also carried out by keeping the particle size, free stream temperature, and velocity constant, but varying the metal surface temperature. The surface temperature was controlled by varying the amount of coolant that impinges on the backside of the plate (Figure 4.1). The more coolant that hit the coupon, the cooler it was. The backside of the thin coupon ranged between 600 to 1000°C while the free stream was at a constant 1200°C. The observed trend here was that the cooler the coupon was, the lower the capture efficiency. This is a trend that has also been observed in other experiments.

The goal of the experiments conducted on a flat plate for this paper is to mimic these observations. Particles made from polymer materials replace the coal ash particles used by Crosby et al. as described in Chapter 2. This will allow similar experiments to be conducted at temperatures that are more reasonable for laboratory settings.

4.2 Geometry of Flat Plate

Since the goal of this experiment is to mimic the experiment by Crsoby et al. [14], the setup is similar to that of Figure 4.1. Hot particle laden flow approaches a 1” coupon angled at 45 degrees from the normal. It should be noted that although the sample is 1” in diameter (see Figure 3.2), the holder is a square that measures 1.25” on each side.

Therefore, any calculations that involve target diameter (2.4) will use 1.25” for this value. The main difference in this setup and that of Crosby et al. is that this setup has the coupon totally immersed in the flow instead of a 1” jet impinging on the surface. The coupon is still made of stainless steel and cooled by a controlled jet that impinges on the backside. Varying the amount of coolant that goes into the system determines the front side surface temperature (Figure 3.5). The sample can be removed from the holder after deposition has occurred for analysis. The deposit laden sample is scanned multiple times under a profiler in order to find the total mass that has become deposited (Equation (3.1). A schematic of the setup is given in Figure 4.2.

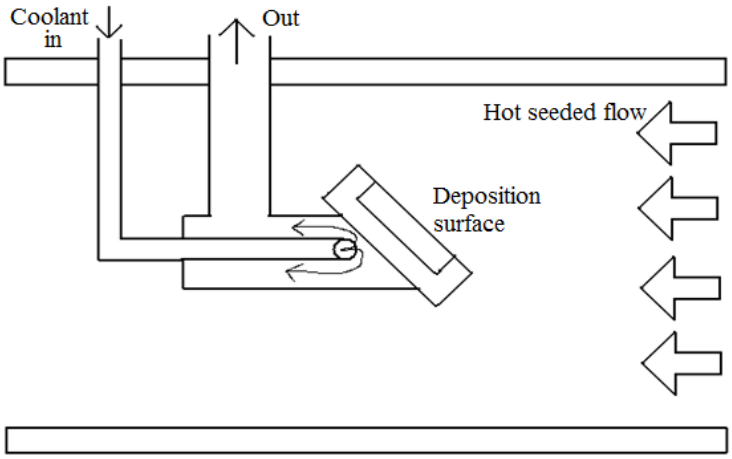

Figure 4.2. Schematic of the flat plate test setup

And a photograph of the rig at the same view is given in Figure 4.3.

Figure 4.3. Photograph of the rig for the flat plate test

Note the location of the 45° angled plate in both Figure 4.2 and Figure 4.3 as hot particle laden flow comes from the left. This setup was constructed to be as similar as possible to that of the Crosby et al.'s as shown in Figure 4.1. The only significant difference in the setup is that this experiment has the coupon completely immersed in the hot flow. The coupon is in the middle of a round pipe that measures 4" in diameter. Windows were installed on each side in the test section so the surface could be viewed during the test. A labeled photograph of the modular combustor rig setup for this experiment is shown in Figure 4.4.

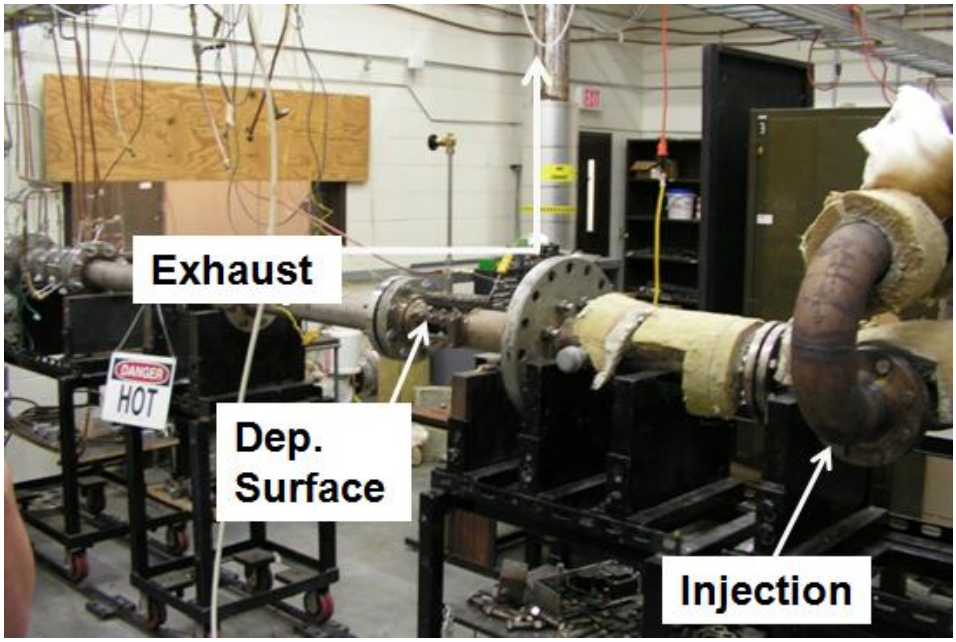

Figure 4.4. Labeled photograph of rig setup for the flat plate experiment

Particles are introduced into the flow through a spray nozzle that injects a mixture of particles suspended in alcohol. The particles are carefully mixed into a solution that is comprised of 1% solid particles and 99% isopropyl alcohol. This is done for two reasons: first, it breaks the particles up in the flow field so they do not form clumps (see Figure 4.12); and second, it allows for easier metering of the injection rate. In order to meet the proper assumptions, the alcohol spray must be completely evaporated and the suspended particles must reach thermal equilibrium before reaching the deposition surface. In this flat plate setup, the injection site is about 1.5 meters away from the surface (Figure 4.4) and flow takes about one full second to reach it. The time constants associated with

evaporation and heat transfer into the particle/spry mixture are all on the order of milliseconds. Time constants associated with fluid forces on the particles are also on the order of milliseconds. This means that the particles have reached fluid and thermal equilibrium with the surrounding flow prior to surface impact.

The spray injector nozzle is manufactured by Delavan, 4.0 liters/hr, type B solid cone, with a 90° spray angle. The particles are injected in a 1% by weight mixture that ends up giving a particle mass flow fate on the order 4.5e-5 kg/s. This spray can be turned on and off with a switch and the mass of particles that end up being injected can be known to an accurate degree. Figure 4.5 is a picture of what the spray nozzle looks like. For this experiment, it is located inside the highly turbulent T section labeled 'Injection' in Figure 4.4.

Figure 4.5. Photograph of spray injection nozzle

After the windowed test section that houses the deposition surface (Figure 4.3) the hot particle laden air is exhausted up a chimney and exits into the atmosphere (Figure 4.4). This is an open loop system as the air is not recycled. It is not feasible to use a closed loop system here because the particle concentration in the air would become unknown. The concentration of particles in the air flow is essential for determining the particle loading factor (PLF, Equation (2.5).

One assumption is this experiment is that the particles are evenly distributed throughout the test section. This is important because the particle concentration

approaching the surface needs to be known. In order to check for this, a planar laser sheet perpendicular to the flow was introduced through the side window just upstream of the surface (Figure 4.3. Photograph of the rig for the flat plate test. The planar laser illuminates the particles are they pass through and the general distribution can be inferred. Figure 4.6. shows two photographs of the planar laser illuminating the area just ahead of the deposition surface. The left photograph is when the particle injector is turned off and the right is when there are particles in the flow. Because the particles are not congregated in just one part of the test section, it can be inferred that the particles are evenly distributed about.

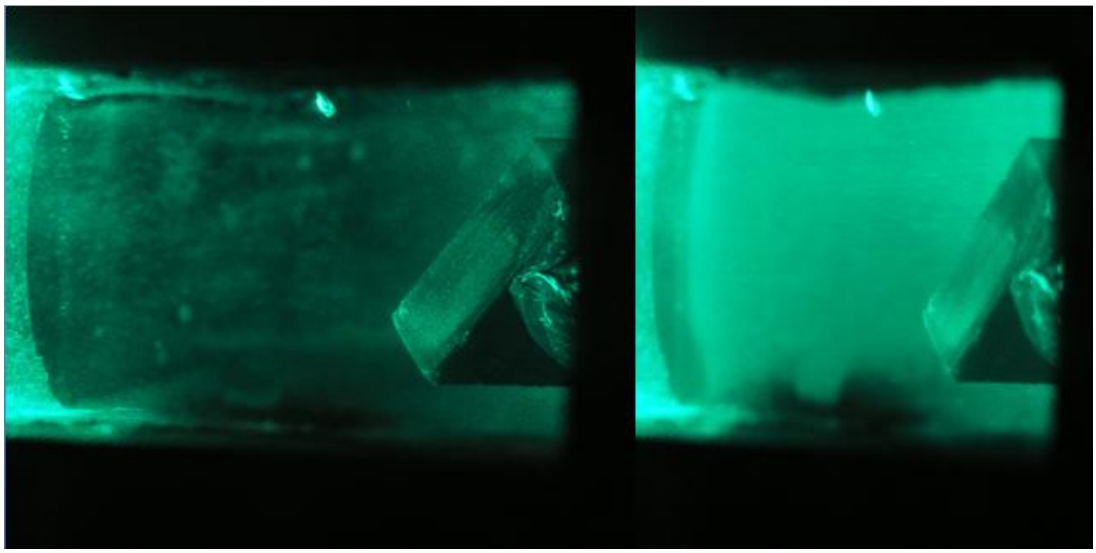

Figure 4.6. A planar laser light sheet showing visually the uniform distribution of the particles just upstream of the flat plate

4.3 Experimental Plan

The central idea is this set of experiments is to mimic the results obtained by Crosby et al. [14] in order to validate the particle substitution method outlined in Chapter 2. The two parameters that will be varied here are the free stream temperature and the metal surface temperature. These two temperatures have been made non-dimensional in the forms of T_1^* and T_2^*, as defined in Equations (2.2) and (2.3) respectively.

Both PVC and Teflon particles were used in this experiment. By matching T_1^*, the free stream temperatures are much lower because the melting point is much lower. In addition to matching the non-dimensional temperatures, the particle momentum Stokes number has also been matched through the velocity.

For the first series of experiments, there was no backside cooling. The only variable was the hot free stream gas temperature (non-dimensional via T_1^*). Because there was no cooling, it was assumed that the surface metal temperature was equal to that of the free stream. In reality, the surface temperature would be slightly less than this due to conduction to the outside of the test section, but this was thought to be negligible. Because PVC and Teflon were used, two sets of experiments were conducted here. In each test, the free stream temperature was varied five times. Table 4.1 and Table 4.2 outline the experimental plan for these two tests. The temperature and flow conditions for these experiments are in the right two columns.

Table 4.1. Experimental matrix for PVC deposition on flat plate with no cooling

Crosby's Free Stream Temperature (K)	**Crosby's Fluid Velocity (m/s)**	**Non-Dimensional Temperature, T_1^* (Both)**	**Particle Momentum Stokes Number**	**Free Stream Temperature (K)**	**Velocity (m/s)**
1133	170	0.672	0.118	361	2.6
1239	170	0.734	0.111	395	2.6
1293	170	0.766	0.108	402	2.6
1347	170	0.798	0.105	429	2.6
1456	170	0.863	0.100	464	2.6

Table 4.2. Experimental matrix for Teflon deposition on flat plate with no cooling

Crosby's Free Stream Temperature (K)	**Crosby's Fluid Velocity (m/s)**	**Non-Dimensional Temperature, T_1^* (Both)**	**Particle Momentum Stokes Number**	**Free Stream Temperature (K)**	**Velocity (m/s)**
1133	170	0.672	0.118	405	4.7
1239	170	0.734	0.111	443	4.7
1293	170	0.766	0.108	462	4.7
1347	170	0.798	0.105	481	4.7
1456	170	0.863	0.100	520	4.7

In the second half of the flat plate experiments, the free stream temperature is kept constant while varying the metal surface temperature. This temperature was controlled by varying the amount of coolant that impinges on the backside of the coupon. A thermocouple on the backside was used to calibrate the front side temperature, as described in Figure 3.5. For these experiments, T_1^* and the Stokes number were matched from Crosby et al.'s experiment and held constant. $T_1^* = 0.75$ and Stk = 0.11. T_2^* was varied by changing the surface temperature. Due to limitations in the cooling scheme, it was not possible to exactly match the full range of T_2^*, therefore the largest possible range was covered instead. Table 4.3 and Table 4.4 give the experimental matrices for the experiments with backside cooling for PVC and Teflon respectively.

Table 4.3. Experimental matrix for PVC deposition on flat plate with backside cooling

Crosby's Free Stream Temperature (C)	Crosby's Front Side Temperature (C)	Crosby's Velocity (m/s)	Crosby's T_2^*	PVC T_2^*	Stokes Number	Free Stream Temperature (C)	Front Side Temperature (C)	Velocity (m/s)
1090	1090	170	0.84	0.92	0.11	173	173	2.6
1090	1019	170	0.72	0.75	0.11	173	162	2.6
1090	919	170	0.58	0.64	0.11	173	146	2.6
1090	852	170	0.52	0.55	0.11	173	136	2.6
1090	780	170	0.45	0.49	0.11	173	126	2.6

Table 4.4. Experimental matrix for Teflon deposition on flat plate with backside cooling

Crosby's Free Stream Temperature (C)	Crosby's Front Side Temperature (C)	Crosby's Velocity (m/s)	Crosby's T_2^*	Teflon, T_2^*	Stokes Number	Free Stream Temperature (C)	Front Side Temperature (C)	Velocity (m/s)
990	990	170	1.00	0.76	0.11	173	173	4.7
990	959	170	0.93	0.85	0.11	173	162	4.7
990	918	170	0.85	0.89	0.11	173	146	4.7
990	891	170	0.81	0.93	0.11	173	136	4.7
990	864	170	0.76	0.98	0.11	173	126	4.7

There is also the need to match the particle loading factor (PLF) as defined in Equation (2.5). For the first series of experiments with no backside cooling the PLF was 96 ppm-hr and for the series with cooling the PLF was 110ppm-hr. In real turbines, PLFs on this scale amount to approximately 5000 hours of operation. For these experiments, the spray nozzle is turned on for about 10 minutes, thereby exposing the surface to 10 minutes of particle laden flow. Experiments are much shorter (5000 hours to 10 minutes) because particle concentrations are much higher (0.02ppm to 400ppm). Because the mass flow rate of solid particles introduced into the system are known and it is introduced for a specified amount of time, the mass of particles injected into the system can be known. This number makes up the denominator of the capture efficiency (Equation (2.6).

4.4 Results and Discussion

Experimental results for both the series with and without the cooled surface are presented here. After each test, the section was allowed to cool and the circular sample was removed from the holder. The surface was scanned using the profiler and the amount of deposition was determined by averaging 20 of the roughness scans. The experiment was setup to mimic results by Crosby et al. [14], so these results are directly compared to the published results.

First, the results from the no cooling series where just the free stream temperature was varied are presented in Table 4.5.

Table 4.5. Experimental results for PVC and Teflon for the no cooling series

Non-Dimensional Temperature, T_1^*	**PVC % Capture Efficiency**	**Teflon % Capture Efficiency**
0.672	0.12	0.085
0.734	0.61	0.11
0.766	0.91	0.176
0.798	1.4	0.37
0.863	3.51	0.736

These results can be graphed along with the published results from Crosby et al.'s experiment that used real coal ash. This graph is given in Figure 4.7. Free Stream Temperature vs Capture Efficiency for PVC and Teflon compared to coal ash

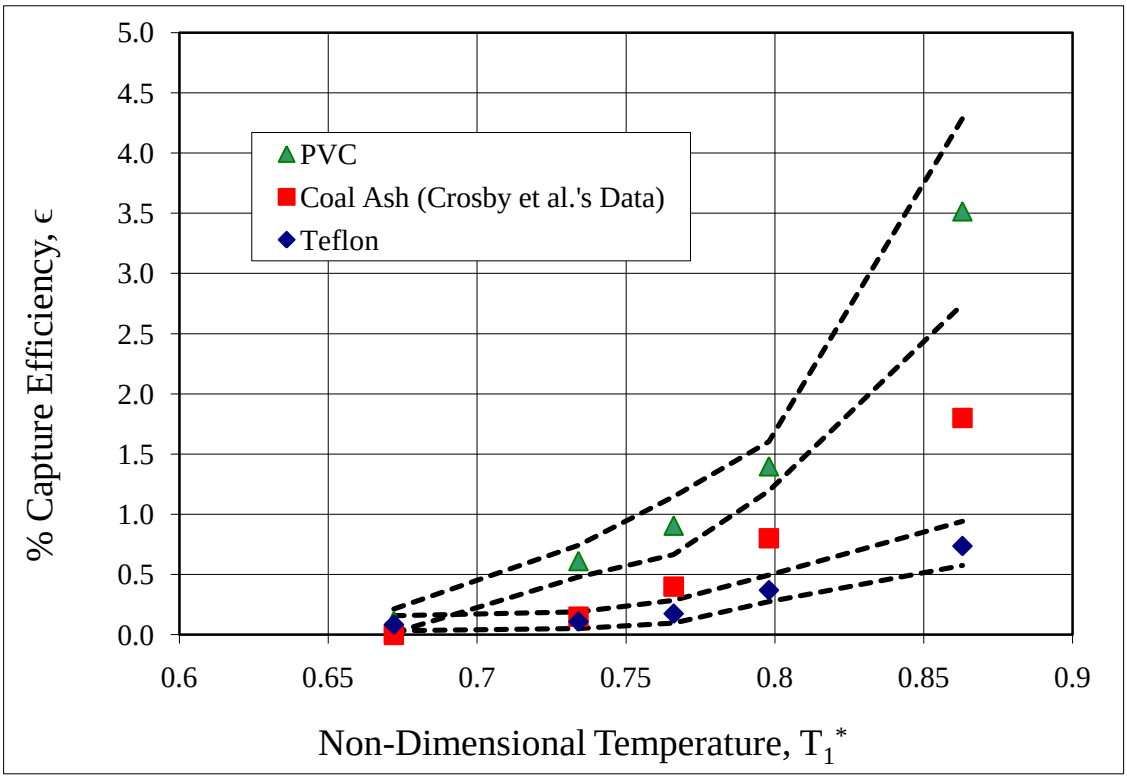

Figure 4.7. Free Stream Temperature vs Capture Efficiency for PVC and Teflon compared to coal ash

The dashed lines on the PVC and Teflon data are error bars that represent $\pm$ 1 standard deviation. This standard deviation is from the 20 surface scans. It is shown that all materials demonstrate an exponential relation between capture efficiency and free stream temperature as the temperature approaches the melting point ($T_1^* = 1.0$). Although they do not fall on the same line, the trend is the same. They are also on similar levels, so it is likely that similar physics are occurring between the different materials. Reasons for these data points not coinciding are unknown, but must have something to do with the chemistry of the particulate material. Detailed reasons for this discrepancy are not discussed in this study.

Next, results from the series with backside cooling are also presented. For this set of experiments, the free stream temperature is held constant and the surface temperature is manipulated by altering the coolant flow. Table 4.6 summarizes these results.

Table 4.6. Experimental results for PVC and Teflon for the series with cooling

PVC, T_2*	PVC % Capture Efficiency	Teflon, T_2*	Teflon% Capture Efficiency
0.49	0.46	0.76	0.24
0.55	0.49	0.85	0.18
0.64	0.56	0.89	0.16
0.75	0.73	0.93	0.13
0.92	1.07	0.98	0.09

Again, these results can be graphed in direct comparison to results published by Crosby et al. Error bars again represent $\pm$ 1 standard deviation from the mean. Figure 4.8 shows the comparison between materials.

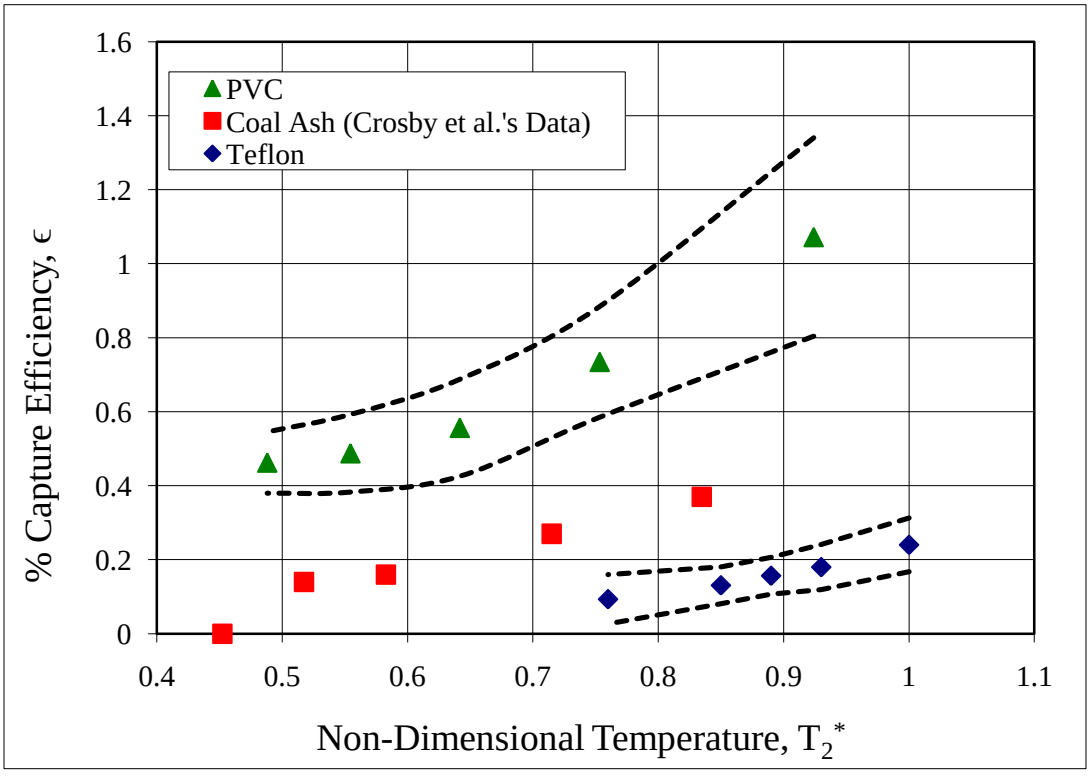

Figure 4.8. Surface temperature vs capture efficiency for PVC, Teflon, and coal ash

Again, similar trends across the board are seen here. A lower T_2^* means more cooling and a cooler surface. So the important lesson from this series is that a cooler surface results in less deposition. The lines still do not coincide, but differences can be attributed to more complex material properties that were not considered in this study.

In addition to measuring the capture efficiency, an effort to describe these trends qualitatively has been undertaken. A scanning electron microscope (SEM) was used to take close up images of the surfaces after deposition of both Teflon and PVC. All images are from the second series where cooling was used to lower the surface temperature while keeping the free stream temperature and velocity constant. Figure 4.9, Figure 4.10, Figure 4.11, Figure 4.12 are SEM images of Teflon at $T_2^* = 0.98$, $T_2^* = 0.85$, PVC at $T_2^* = 0.92$, and $T_2^* = 0.49$ respectively.

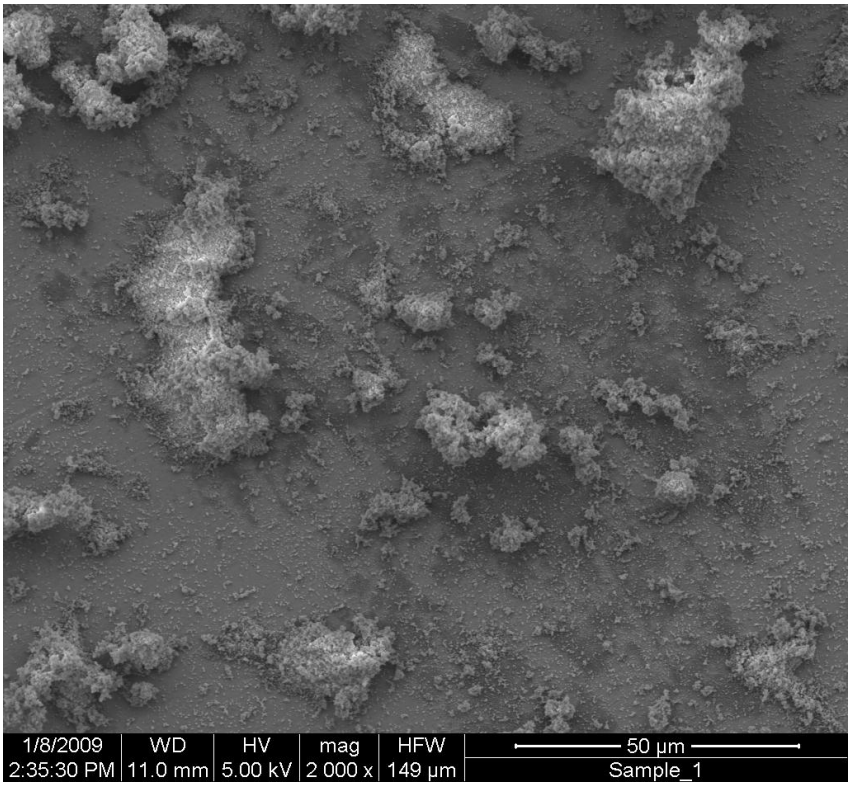

Figure 4.9. SEM image of Teflon when $T_2^* = 0.98$

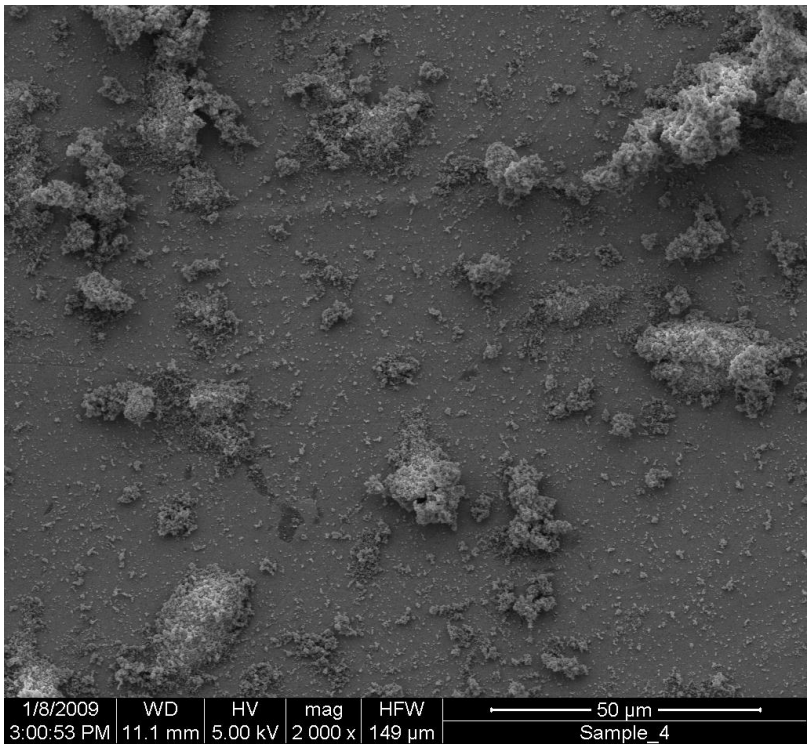

Figure 4.10. SEM image of Teflon when $T_2^* = 0.85$

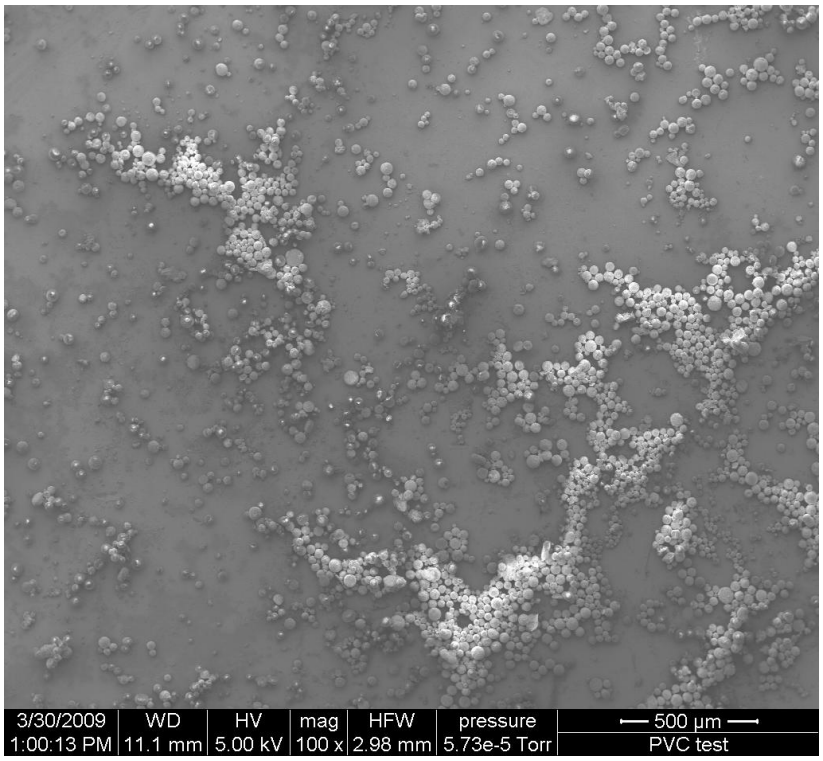

Figure 4.11. SEM image of PVC when $T_2^* = 0.92$

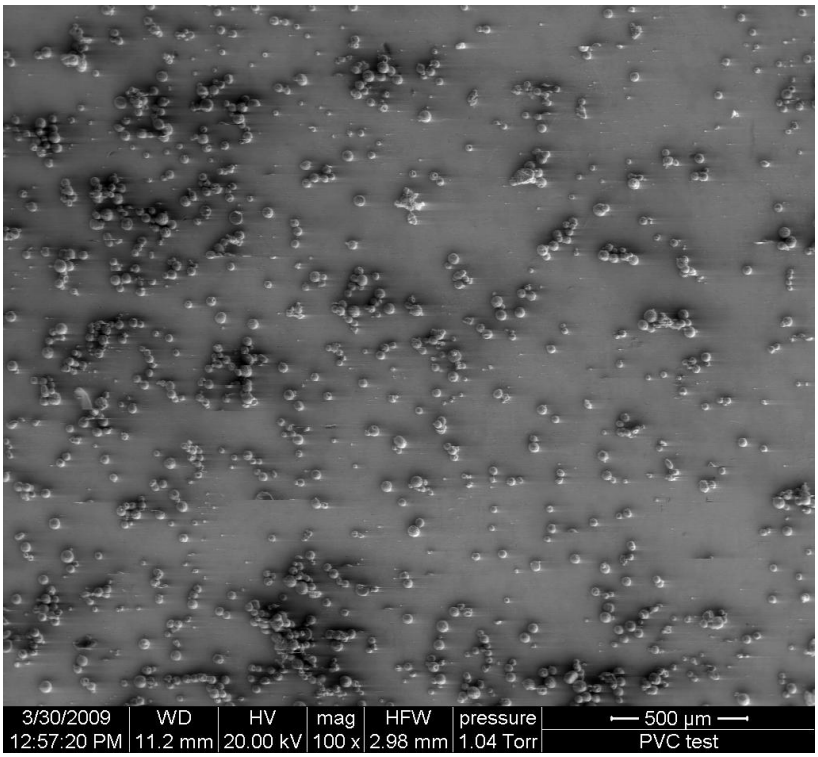

Figure 4.12. SEM image of PVC when $T_2^* = 0.49$

These images are a confirmation of the overall trend observed from the more exact results of capture efficiency. In comparing the two Teflon and the two PVC images, it can be seen that cooling the surface does indeed lower the number of particles that stick to it. These images also provide some insight into how deposition patters form on the surface and could be of interest into future research pursuits.

The particle loading method described in Chapter 2 was tested for repeatability. An assumption for the PLF and scaling method is that the rate at which particles deposit on the surface is more or less constant throughout the deposition phase. For PVC with backside cooling, $T_2^* = 0.75$, the test was allowed to run for a much longer period of time (~50 min) in order to match the total mass of particles that approach the plate in Crosby et al.'s experiment [14]. If the deposition rate is constant then the capture efficiency should not be a function of time nor mass already on the plate. Another way to say this, is that if twice the number of particles approach the plate, then twice the number of particles will become deposited. In this case, the capture efficiency was found to be 0.62%, slightly less than the value expected of about 0.70%. However, this is within the

error bars (Figure 4.8), so there is no strong evidence that deposition rate changes with time. Repeatability is also a major concern, so an extra sample was run for both the no cooling ($T_1^* = 0.766$) and the cooling cases ($T_2^* = 0.64$). Both instances gave results that were within the error bars from the original data point and not more than 10% difference. Although no variability would be ideal, changes within 10% from identical conditions can be considered acceptable for this kind of experiment.

The experiments on the flat plate have established that using polymer particles as a substitute for coal ash is not a perfect method, but it is workable. The deposition characteristics between coal ash and polymer particles do not coincide, but they do share the same trends and on the same level. It was also decided that PVC is a better substitute than Teflon because the PVC particles are more spherical, not as clumpy, and trends with coal ash match better. For this reason, the next set of experiments will only use PVC as the particulate material.

5 Experiments on Leading Edge with Film Cooling

5.1 Geometry of Lead-in Sections

The experiments on the semi-cylindrical leading edge with film cooling and a flat after body used a new setup in the modular combustor rig. The flat plate experiments were conducted with a circular profile in the test section. The experiments on the leading edge call for a rectangular cross section. For this reason, new sections have been designed, fabricated, and installed for this experiment. A 3-D model of the lead-in sections is given in Figure 5.1.

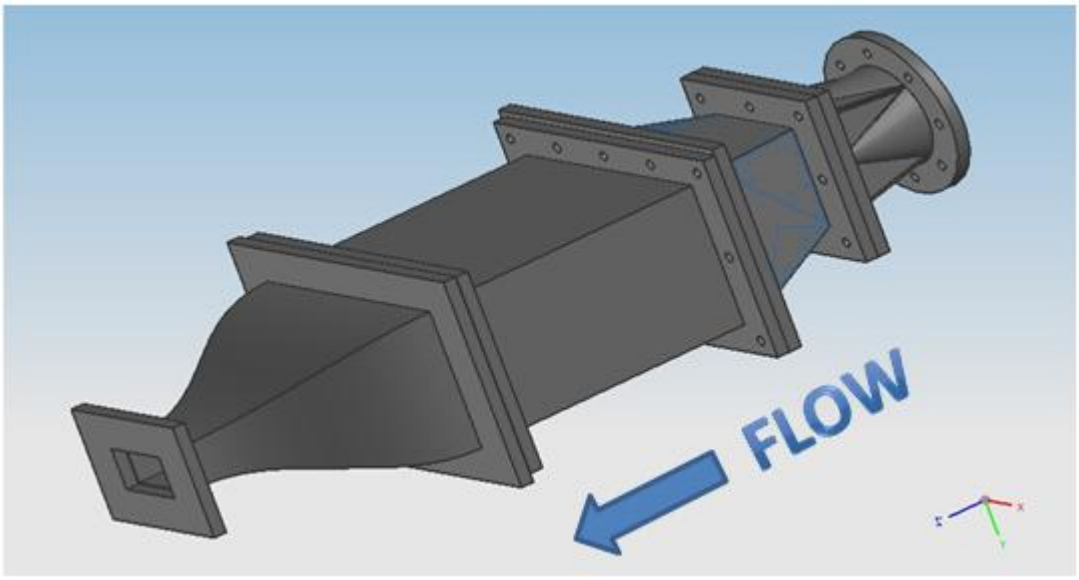

Figure 5.1. 3-D model of the lead-in sections (flow goes right to left)

The first piece of the lead-in sections was made to transition the overall shape of the flow area from circular to square. The far right flange (Figure 5.1) is an 8" circular fitting that connects to the T section of the modular combustor rig (Figure 3.1). As the flow transitions to a square of 8" per side, the flanges also change shape. The next section expands the flow from the 8" square to a large rectangle. This rectangle measures 12" on the vertical and 18" on the horizontal. This expansion also slows the flow down as it enters the setting chamber.

Because the results from this experiment are to be compared to CFD, effort has been taken to best match the incoming flow conditions. One of the hardest fluid dynamic aspects to model in CFD is turbulence. Turbulence is highly unpredictable and can cause tremendous differences from an idealized flow. The lead-in sections were designed with the goal of creating as little turbulence in the test section as possible. Design guidelines for these sections are given by Metha and Bradshaw [30]. This is accomplished by straightening the flow in a settling chamber and accelerating in a contracting section.

The rectangular expansion has the same cross sectional profile as the settling chamber. The settling chamber is the long rectangular section in the middle of Figure 5.1. It is here that the flow is greatly reduced in turbulence as it passes through a series of flow strengtheners. The first device the flow sees is a 1" thick ceramic honeycomb that is made up of 1/8" squares. After the honeycomb, the flow passes through 4 layers of stainless steel screens that become finer as the flow advances. The number of openings per inch of the screens is 16, 26, 26, and 32 respectively. Additionally, the wire diameter for each of these screens is 0.018", 0.0075", 0.0075", and 0.0065". Note that screen #2 and #3 are identical. Each of the screens is spaced 3" apart as well. All flow straightening devices are held taught and compressed into place.

As the flow exits the settling chamber, it enters the contraction section. The contraction section takes the 12" x 18" profile and reduces it down to a 5.3" x 3.5" profile. This is a 12:1 ratio that accelerates the flow. All sides contract according to a fifth-order polynomial. The aspect ratio of the 12" x 18" profile is the same as the 5.3" x 3.5" profile. This smaller rectangular profile is the same as the test section that houses the semi-cylindrical surface.

Since the goal of creating these sections is to reduce the turbulence, the turbulence levels were measured. Turbulence is unsteadiness in a flow and can be expressed as the turbulence intensity (Tu), as given in Equation (5.1).

$$Tu = \frac{u'}{U_\infty} \tag{5.1}$$

Where u' is the root mean square (RMS) of the unsteady part in the flow and U_∞ is the average steady free stream velocity. Only a one dimensional analysis was considered, which is sufficient in this case because the overwhelmingly uniform direction of the flow..

A hot wire was used to measure the unsteady aspect of the velocity. The contracting section was left open to the atmosphere and given 800 SCFM, which translates to an average velocity of 30m/s. A hotwire is a very thin heated wire that very accurate measures changes in resistance as convective heat transfer changes due to velocity fluctuations. Data was taken at 12 kHz for two minutes, which is more than enough to cover the entire dynamic range of unsteady flow. 88 data points were taken all across the outlet section as depicted in Figure 5.2.

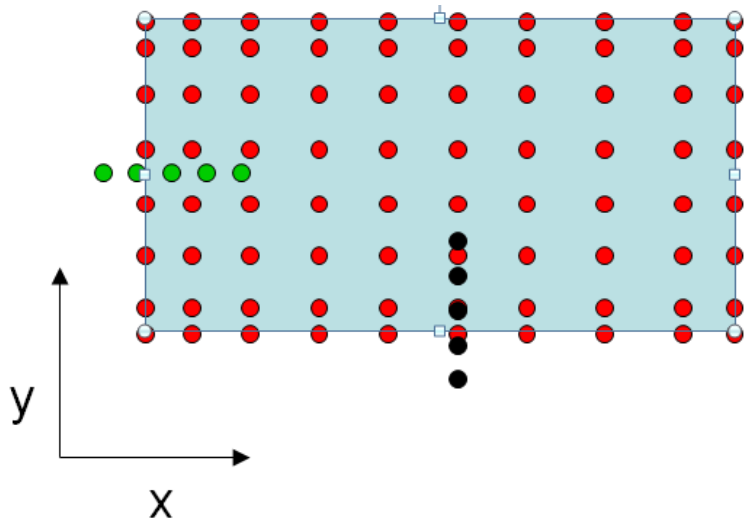

Figure 5.2. Location of data points for hot wire probe

Post processing of the data can give the average velocity at each point, the root mean square of the velocity fluctuations at each point, and thereby the turbulence intensity at each point. Figure 5.3 is a contour map of the contraction section's average velocity at each point as a fraction of the maximum velocity (total average velocity was ~30 m/s). Figure 5.4 plots the RMS value (in m/s) of the unsteady component of the velocity for the same area.

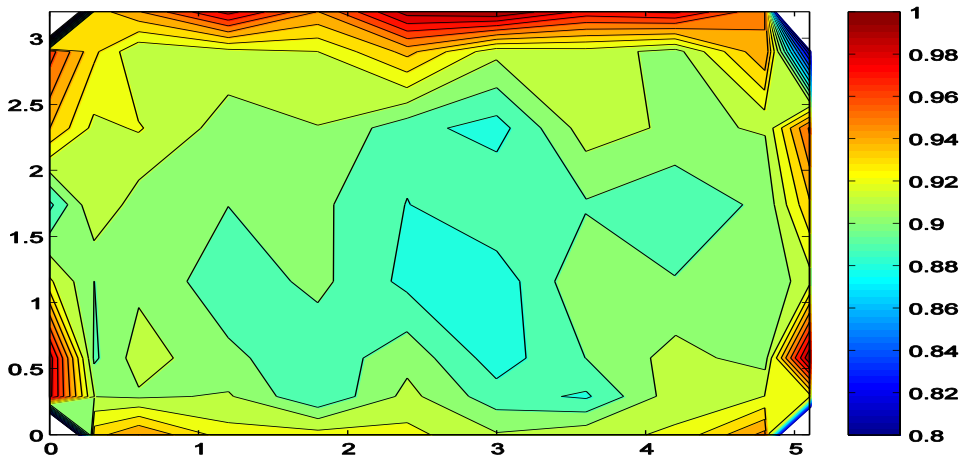

Figure 5.3. Average velocity as fraction of max across the contraction section outlet

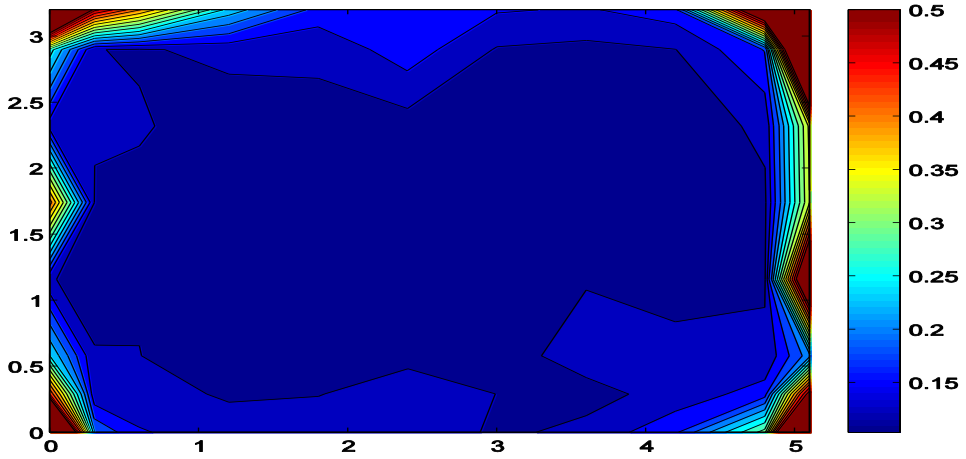

Figure 5.4. RMS of unsteady velocity component (in m/s) across the contraction section outlet

Average steady velocity through the center of the test section did not vary by more than about 5%. The global turbulence intensity was measured to be 1.6%. Estimates for fully developed pipe flow under these conditions with no flow conditioning could be as high as 8%. Using the flow straightening devices and contracting section have greatly reduced the levels of turbulence in the test section.

These sections are capable of being pressurized as well and were designed using the ASME pressure vessel standard [31]. All of the sections here were constructed from 314 grade stainless steel so that they will keep their integrity at high temperatures. The flanges are rated up to the 150 psi standard. All sections (except for the contraction section) are made to be ¼" thick. The contraction section was made with 1/8" stainless steel. Designs are been made to add reinforcements to that section in case future experiments wish to be pressurized. Experiments presented herein have all been done at or near atmospheric conditions.

To be assured that the sections designed are capable of withstanding the temperature and pressure loads desired, a finite element analysis (FEA) has been completed on all parts. Stresses were simulated in 3-D for the worst possible case scenarios. Although the sections will never practically experience such conditions, the FEA stress analysis was done for a temperature of 1000°F and an internal pressure of 10 atm. Under these conditions, the stress levels were comfortably below the yield stress for stainless steel. Strains were also relatively low and within acceptable limits of less than 1%. A sample 3-D strain plot for the rectangular expansion section is shown in Figure 5.5. Physical deformation of the section in the image has been greatly exaggerated. Real nodal displacements were on the millimeter level.

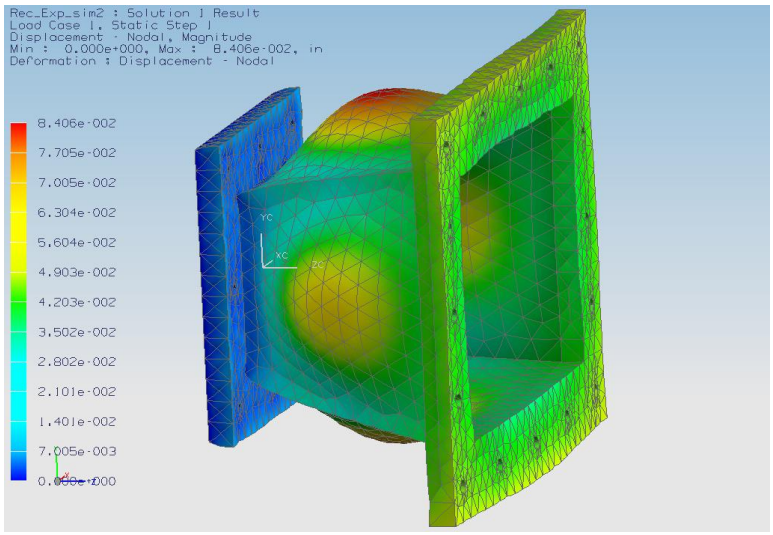

Figure 5.5. FEA strain analysis on the rectangular expansion section

All of the lead-in sections were installed in the modular combustion rig in the CSDL and leak tested. After the test section, the air enters a 4" pipe and is exhausted up the stack and into the atmosphere in the same fashion as the flat plate setup. A photograph of all the sections installed is shown in Figure 5.6.

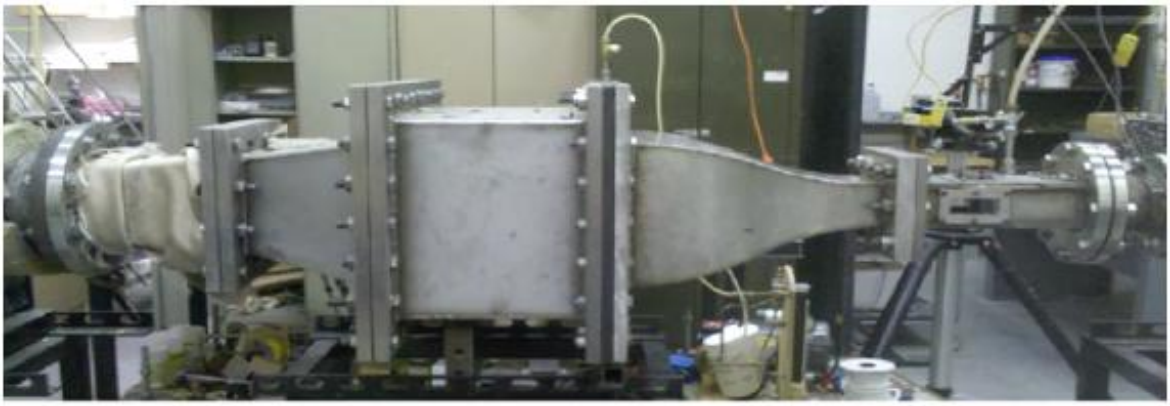

Figure 5.6. Photograph of experimental sections installed at CSDL (flow goes from the left to right)

Because of the fine screens in the settling chamber, the spray nozzle for particle injection could not be located at the T section as shown in Figure 4.4. The particles would clog up the screens resulting in both the particles not reaching the deposition surface and great disturbances to the flow regime. For this reason, the spray nozzle was located just upstream of the contraction section and just after the last screen. A black frame that holds the nozzle in place and the particle feed line can be seen in the middle of Figure 5.6. The spray nozzle points upstream and away from the test section (to the left) as to encourage the greatest dispersion of particles. As with the previous experiment, the alcohol should evaporate within 10 cm and the particles should reach thermal and fluid equilibrium soon after and before impacting the surface.

5.2 Geometry of Test Section and Leading Edge

The rectangular exit from the 12:1 contraction section is the same size (5.3" x 3.5") as the cross-sectional area of the test section. The windowed test section is the rightmost

piece shown in the photograph in Figure 5.6. The test section is the same straight rectangular shape for its 14” of length. In the middle of the test section rests the semi-cylindrical leading edge with a flat after body blade. An image of the CAD model showing a side view of the contraction and test sections is given in Figure 5.7.

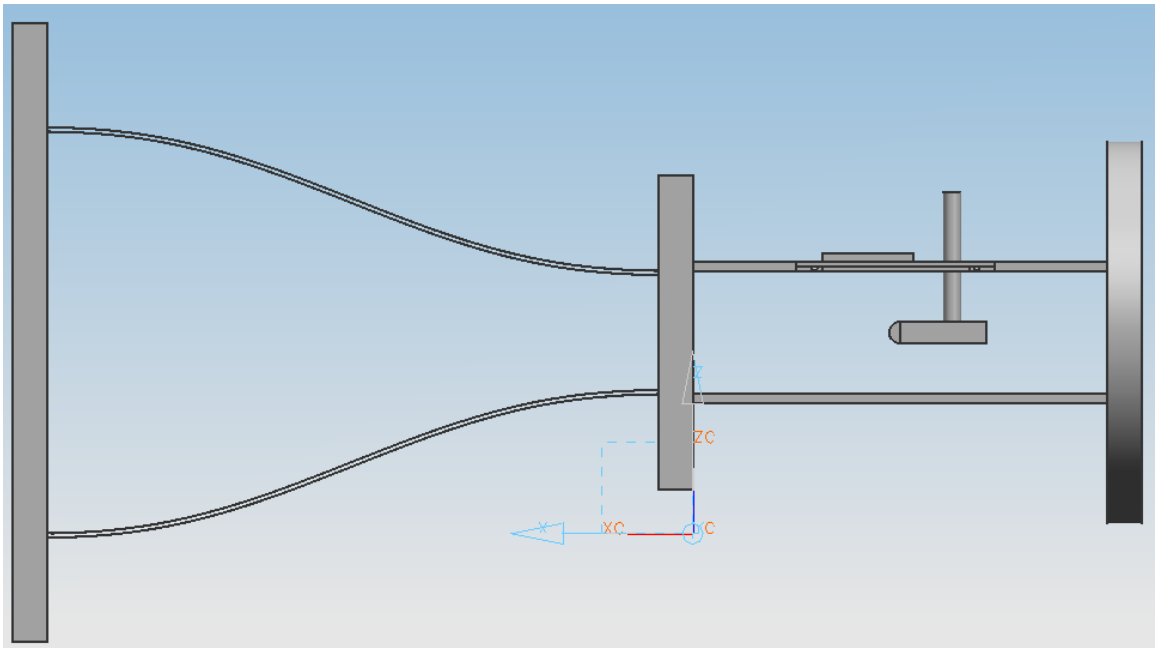

Figure 5.7. CAD side view of contraction and test sections

The test section has been built with two glass windows on the sides to give optical access to the deposition surface. The blade body is hollow to allow coolant air to pass through and out the coolant holes on the leading edge. The body is suspended in the test section only by the coolant feed line as shown in Figure 5.7. The exit of coolant through cooling holes on the semi-cylindrical leading edge allows film cooling to occur. A schematic of this setup as well as a complementary photograph is shown in Figure 5.8 and Figure 5.9 respectively. The IR window is located above the leading edge to allow the IR camera to make surface temperature measurements. The setup is such that only the top half of the leading edge will be seen with the IR camera, but both halves should be similar due to symmetry. The IR window measures 1.25” x 2.5” and is ¼” thick. It is made from Zinc Selenide which is material that allows just the right wavelengths in the infrared spectrum to pass. The window also has anti-reflective coatings on both sides and

is scratch resistant. The leading edge, after body, and inner test section walls were painted black to more resemble black body radiation.

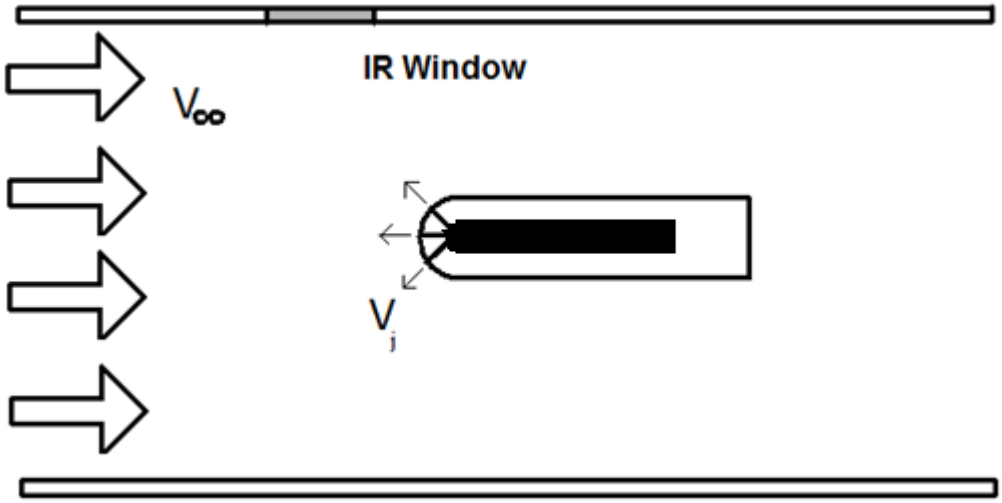

Figure 5.8. Schematic of leading edge geometry with film cooling

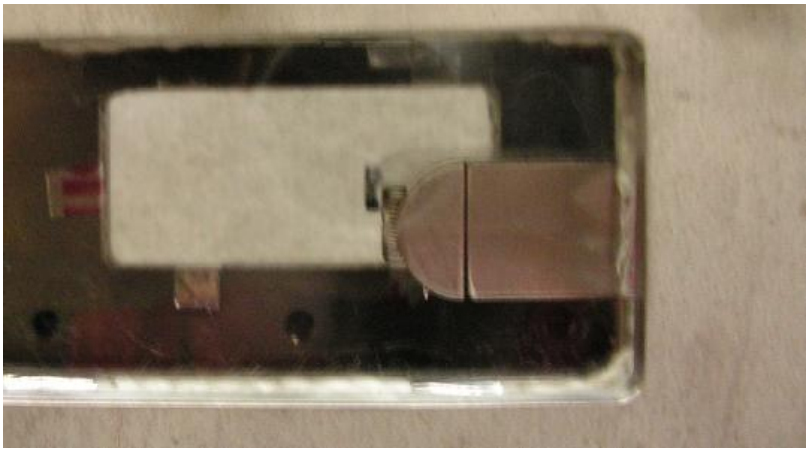

Figure 5.9. Photograph of the leading edge from side through window

The inside of the after body is modeled as a plenum which feeds coolant air from the outside to the cooling holes on the leading edge. Before entering the plenum, the coolant air passes through tubing in an ice bath to reduce the temperature. The greater the difference between T_{∞} and T_{cool}, the better the resolution for the IR results. There is also a thermocouple inside the plenum near the coolant exit. This thermocouple gives the

coolant exit temperature that is part of the cooling effectiveness measurement, given in Equation (3.3). Care was taken to ensure that the interface between eh plenum body and detachable leading edge was sealed and no coolant leaking took place.

The leading edge is 5/8" thick and attaches to the after body by two screws on either side. The coolant holes are 1/32" in diameter with an l/d ratio of 4.5. There are 3 rows of coolant holes of 16, 17, and 16 holes respectively - totaling 49 holes. A photograph of the assembly (not painted) is shown in Figure 5.10 and the detached leading edge with no deposits on it (painted black) is given in Figure 5.11.

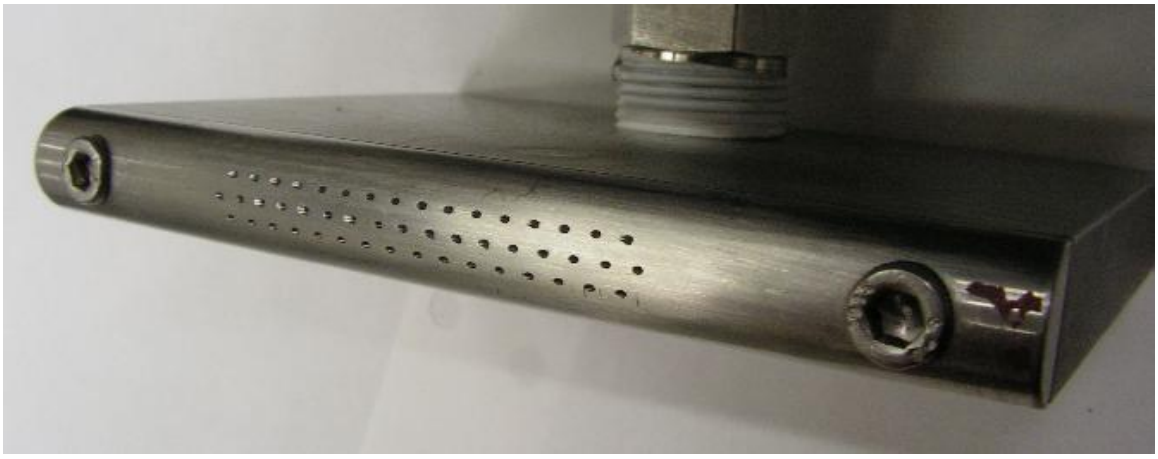

Figure 5.10. Photo of leading edge attached to after body

Figure 5.11. Leading edge with no deposits

The cooling holes are in three rows such that the middle row is at the stagnation point in the flow and the other two rows are located 23° above and below the stagnation point. The holes are also angles 45° normal to the flow along the lengthwise direction of the leading edge. This will give the coolant lateral momentum and will cover more of the surface. The direction of the coolant jet will be noted with the results.

5.3 Experimental Plan

The experiments on this geometry used PVC as the substitute material to ash. Tests were conducted to study the effect of free stream temperature (non-dimensional by T_1^*) and blowing ratio on the capture efficiency. The blowing ration is a non-dimensional measurement of momentum of the coolant jet compared to the incoming momentum of the free stream. The blowing ration (BR) is defined in Equation (5.2).

$$BR = \frac{\rho_{cool}\ U_{cool}}{\rho_\infty U_\infty} \tag{5.2}$$

Where ρ_{cool} and U_{cool} are the density and jet velocity of the coolant and ρ_∞ and U_∞ are the density and velocity of the free stream. The higher the blowing ratio, the more coolant there is and when the blowing ratio equals zero there is no coolant flow. In addition to studying how the free stream temperature and blowing ratio affect the capture efficiency, a comparison of film cooling effectiveness and convective heat transfer before and after deposition was done.

Because these results are to be matched with CFD, the flow conditions need to be as similar as possible. Ideally, the particle momentum Stokes number would be one and the Reynolds number (based on leading edge diameter) would be 32,000. However, this was not possible due to the increased size of the particles (24μm). By setting the Reynolds number to 32,000 the velocity would be greatly increased resulting in a Stokes number of 8. If the Stokes number was set to one, then the velocity would be low and the Reynolds number would be 9,000. Since both of the ideal Stokes and Reynolds numbers cannot be matched simultaneously, a compromise was reached. The velocity would be in between which results in the Stokes number being 3.8 and the Reynolds number being around 18,500. The test matrix for the experiment on the leading edge geometry using this compromise is outlined in Table 5.1.

Table 5.1. Test matrix for deposition in leading edge geometry.

Blowing Ratio	Non-Dimensional Free Stream Temperature, T_1^*	Particle Stokes Number	Reynolds's Number	Free Stream Temperature, (K)	Free Stream Velocity, (m/s)
0	0.71	3.8	21019	378	29
0	0.80	3.8	18394	426	32
0	0.89	3.8	16666	474	35
1.0	0.71	3.8	21019	378	29
1.0	0.80	3.8	18394	426	32
1.0	0.89	3.8	16666	474	35
2.0	0.71	3.8	21019	378	29
2.0	0.80	3.8	18394	426	32
2.0	0.89	3.8	16666	474	35
3.0	0.71	3.8	21019	378	29
3.0	0.80	3.8	18394	426	32
3.0	0.89	3.8	16666	474	35

The free stream velocity in the right column and the Reynolds number varies due to make up for changes in the viscosity and density at different temperatures. The temperature covers a range of 100°C and the blowing ratio goes up to 3.0. Cases at a blowing ratio of zero (cooling turned off) were also done as a control. It should be noted that these are at much higher velocities and Stokes numbers than the experiments on a flat plate. The flat plate experiments used a Stokes number of 0.11, and here that number is 3.8.

The surface was be exposed to particulate loading such that the particle loading factor (PLF, Equation (2.5) is equal to 100ppm-hr. This represents approximately 500 hours in a real turbine, assuming particle concentration of 0.02ppm. At the higher concentration on this geometry, exposure time lasts between 12-15 minutes; depending on the air density and velocity.

Film cooling effectiveness and heat transfer as be measured before and after some of the test cases to determine the effect particle deposition has on those parameters. Convective heat transfer has been made non-dimensional by the Stanton number. This comparison could not be done for all cases because they require use of the IR camera which was not always available.

5.4 Performance before Deposition

Before the leading edge was exposed to particulate laden hot air, the film cooling effectiveness and convective heat transfer were measured using the methods described in Chapter 3. In order to better match cooling effectiveness results with CFD efforts, the leading edge was made of plastic material. The plastic material cannot withstand the high temperatures needed for deposition, so the free stream temperature was limited to 60°C. This should not affect the results too much because film cooling effectiveness is non-dimensional and should only be a function of geometry and blowing ratio.

Figure 5.12 is a series of six raw images from the IR camera of the plastic model. The top left image is at a blowing ratio of 0.5, top right is 1.0, and this pattern continues to 3.0 in the bottom right. Hot flow goes from the bottom to the top of each individual image and coolant is being injected at 45° from the right to the left. In each individual image, the bottom line of holes (dark spots) is the stagnation point and the upper line of holes is the off-stagnation cooling holes at 23°.

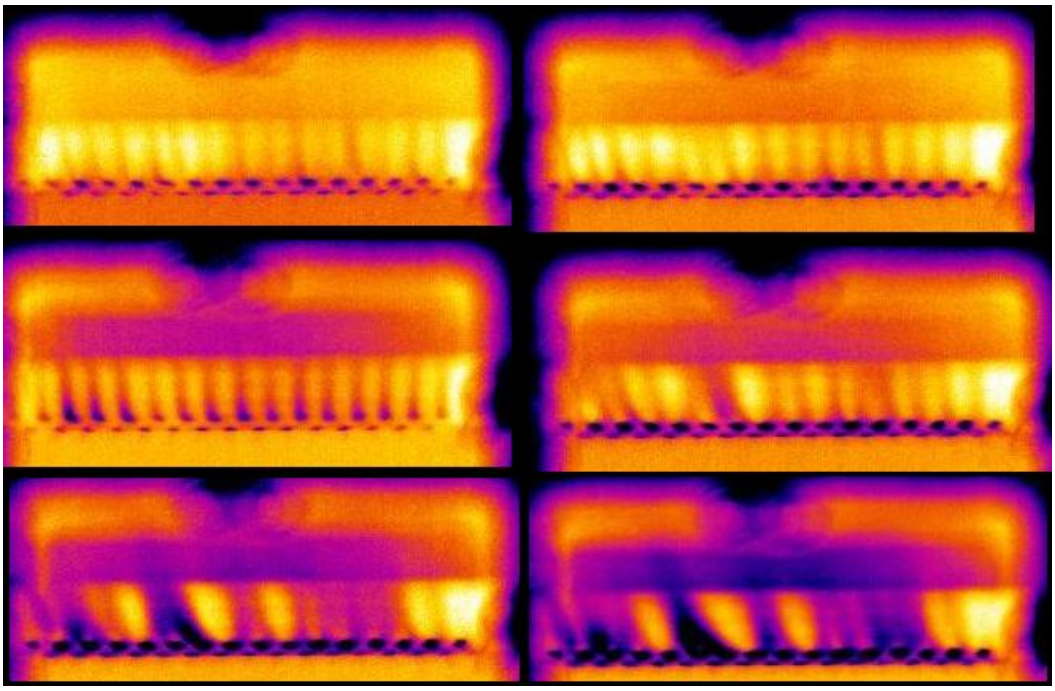

Figure 5.12. Raw IR images on plastic model for BR = 0.5 - 3.0

The raw data from the IR camera and its software can be saved as a comma separated variable file and sent to Matlab for post processing and data reduction. A copy of the Matlab program that does this is in the Appendix. The same data from Figure 5.12 has been reduced such that only the blade is shown and the contour plots represent the effectiveness. Figure 5.13 gives the corresponding effectiveness for four colors on the contour plots. Because effectiveness is non-dimensional, the same key applies to all contour plots. Even though the same color between individual contours plots means the same effectiveness, it does not necessarily mean the same surface temperature. This is because higher blowing ratios tended to have lower coolant jet temperatures. Figure 5.14 gives the contour plots for the plastic model; each image in the figure corresponds to same data as in Figure 5.12.

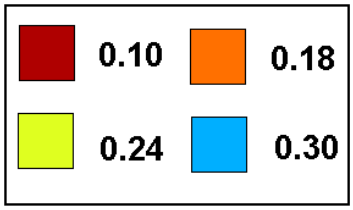

Figure 5.13. Color key for effectiveness contour plots

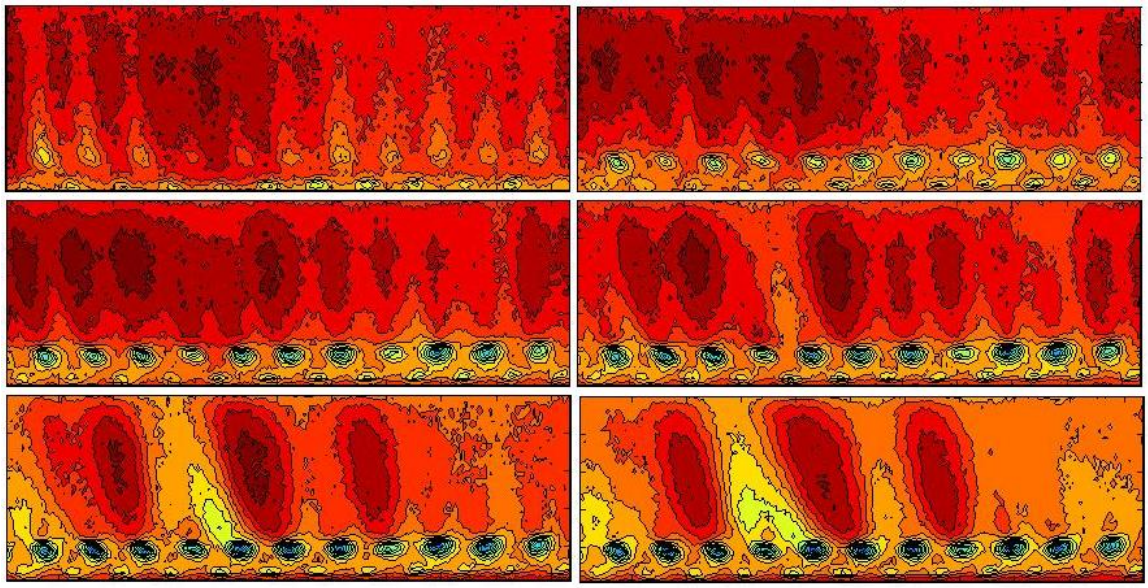

Figure 5.14. Contour plots for plastic model for BR = 0.5 – 3.0

This data can then be translated into adiabatic effectiveness as a function of angle from stagnation. Θ goes from zero (stagnation) to 90° (where the semi-cylindrical geometry ends) and is more clearly depicted in Figure 3.6. Figure 5.15 gives adiabatic effectiveness for the plastic model at various blowing ratios.

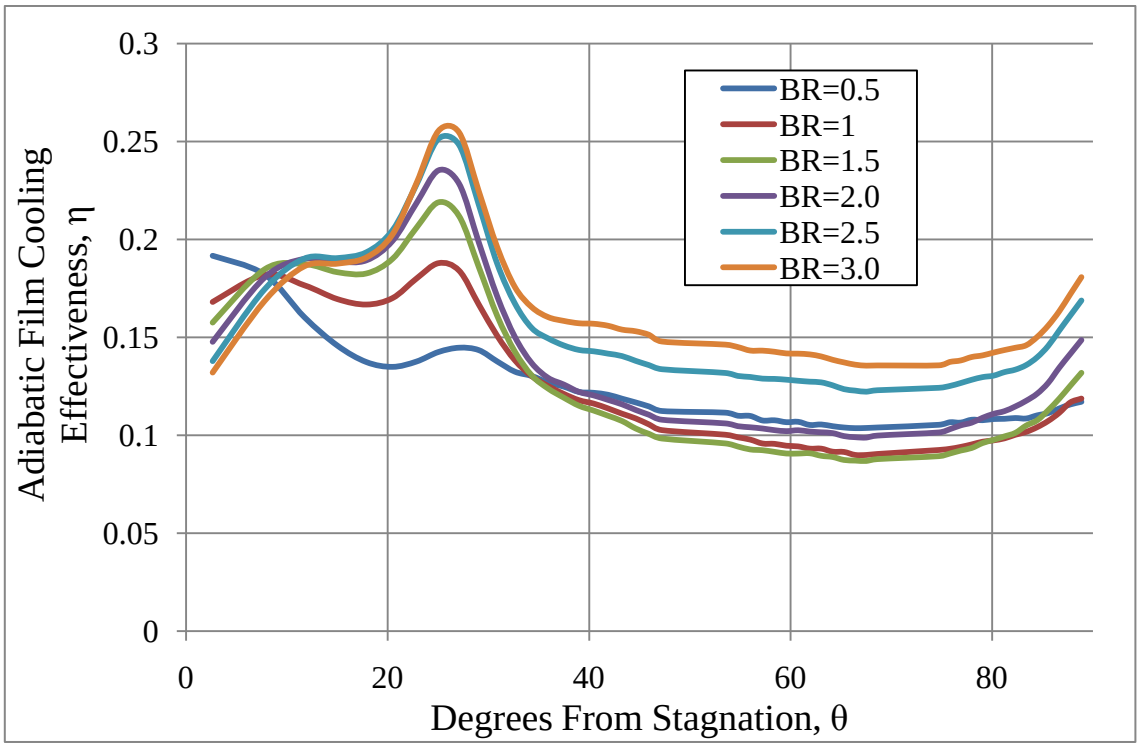

Figure 5.15. Cooling effectiveness as function of angle at various blowing ratios on the adiabatic plastic model

A noticeable feature for all blowing ratios is the peak at 23°. This is the location of the off-stagnation coolant holes. The extra injection of coolant cools the surface at 23° and gives a rise to the cooling effectiveness. The other noticeable trend is that cooling effectiveness rises with blowing ratio. This makes sense because the more coolant there is, the cooler the surface will become.

The effectiveness data was also taken on the steel model before deposition. Because deposition can only occur at higher temperatures, the cooling characterization needs to be done without deposition also at high temperatures. This will allow a one to one comparison of the cooling characterization before and after deposition. Figure 5.16 gives the raw IR images on the metal leading edge at various blowing ratios. The top left

image is at a blowing ratio of 0 (as a reference), top right is 1.0, bottom left is 2.0, and bottom right is 3.0. T_∞ was set to 426K and the oncoming air velocity was at 32 m/s. Coolant jet temperature varied between 315K and 331K.

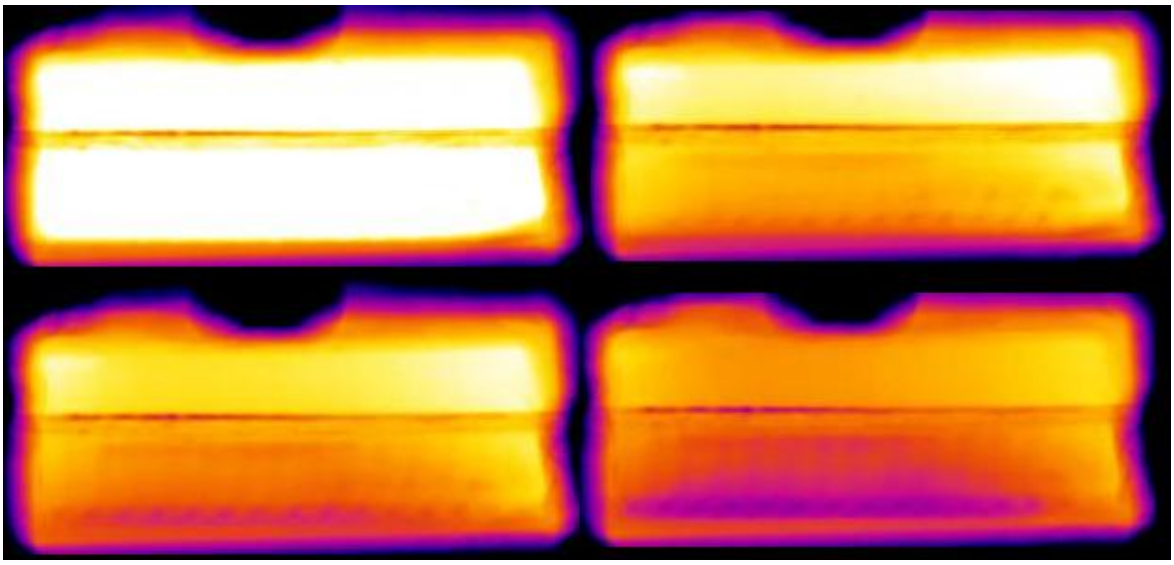

Figure 5.16. Raw IR images for steel leading edge at various blowing ratios

Similarly as before, this raw data can be processed into contour plots, as shown in Figure 5.17. Additionally, Figure 5.13 can be used as a color key for effectiveness levels. The top image is at a blowing ratio of 1.0, the middle is 2.0, and the bottom is 3.0. A contour plot of blowing ratio equal to zero is not shown because effectiveness is not defined when there is no cooling. If T_∞ is the same as T_{cool}, then denominator in Equation (3.3) goes to zero. The data shown here is of adiabatic effectiveness because the method for method for calculating out conductive losses discussed in Chapter 3 has been used. The most noticeable difference between the plastic and metal surfaces is that streaks of coolant do not appear on the metal surfaces. This is due to the conductive nature of metal and high temperature gradients are not sustainable. Coolant holes are still visible, but not as pronounced as with the plastic model.

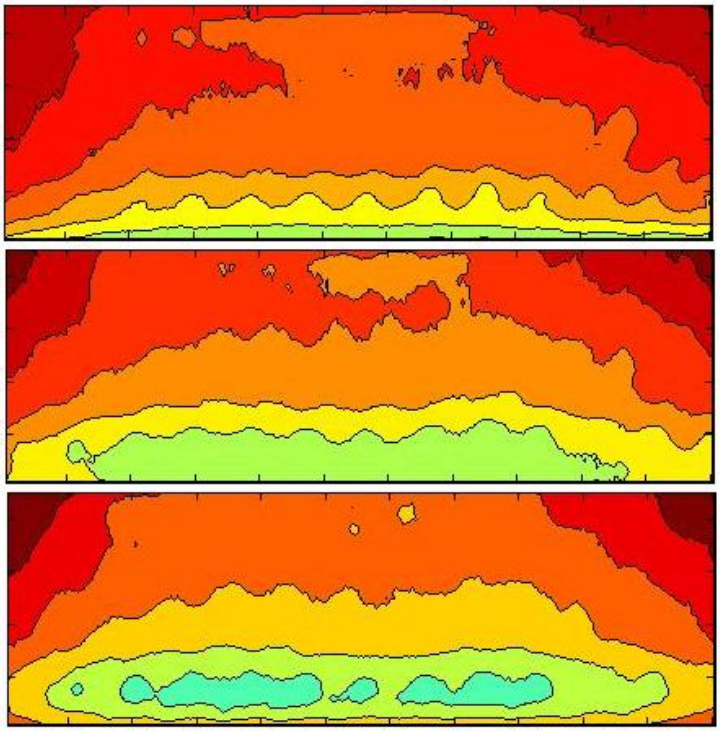

Figure 5.17. Contour plots for steel leading edge for blowing ratios 1.0 – 3.0

As before, the adiabatic cooling effectiveness can be plotted as a function on angle at various blowing ratios. This is shown in Figure 5.18.

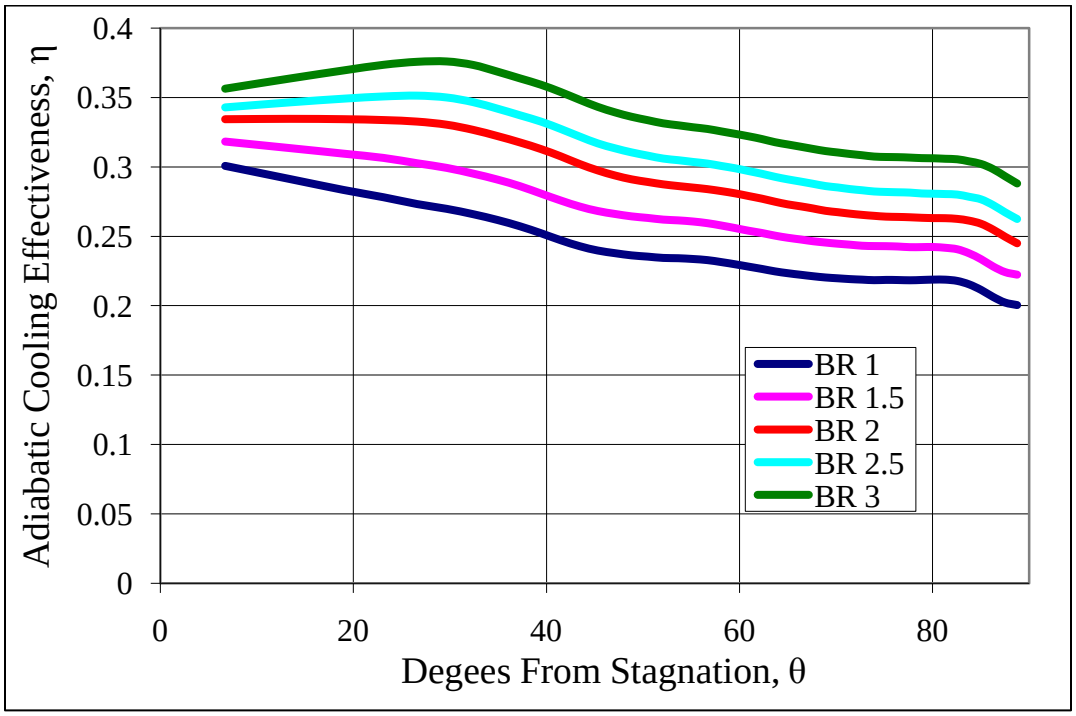

Figure 5.18. Effectiveness vs angle on metal surface at various blowing ratios

There is still a maxima at 23°, but not as pronounced as with the plastic model. Again, this is because the surface is more conductive. The trend of increased cooling effectiveness with increased blowing ratio is also observed here. The overall level of cooling effectiveness in Figure 5.18 (metal) is substantially higher than Figure 5.15 (plastic). Ideally they would have the same average, but the discrepancy is most likely due to inadequacy in the adiabatic correction described in Chapter 3. It was assumed that the entire blade experiences constant surface heat flux, but this is probably faulty. The surface heat flux towards the front of the blade (near stagnation) would be higher than further down the flat after body or the rear wall. Film cooling performance on the metal surface has been summarized in Table 5.2.

Table 5.2. Cooling performance on steel leading edge with no deposition

T_∞, (K)	Blowing Ratio	T_{cool}, (K)	Average Surface Temperature, (K)	Film Cooling Effectiveness, η	T_2^*
426	1.0	331	403	0.24	0.824
426	1.5	329	400	0.27	0.803
426	2.0	324	395	0.305	0.775
426	2.5	320	391	0.33	0.754
426	3.0	315	388	0.345	0.736

In addition to the surface temperature, the convective heat transfer has also characterized as a function of angle at various blowing ratios. Here the free stream velocity was 32 m/s and the temperature was 426 K. The method for finding the convective heat transfer coefficient, h, is outlined in Chapter 3. The convective heat transfer coefficient is presented as the non-dimensional Stanton number (Equation (3.8). These results for blowing ratios of 1.0, 2.0, and 3.0 are given in Figure 5.19. There are two general trends here. First, increasing the blowing ratio will increase convective heat transfer. Second, heat transfer is highest near stagnation (0°) and decreases with angle.

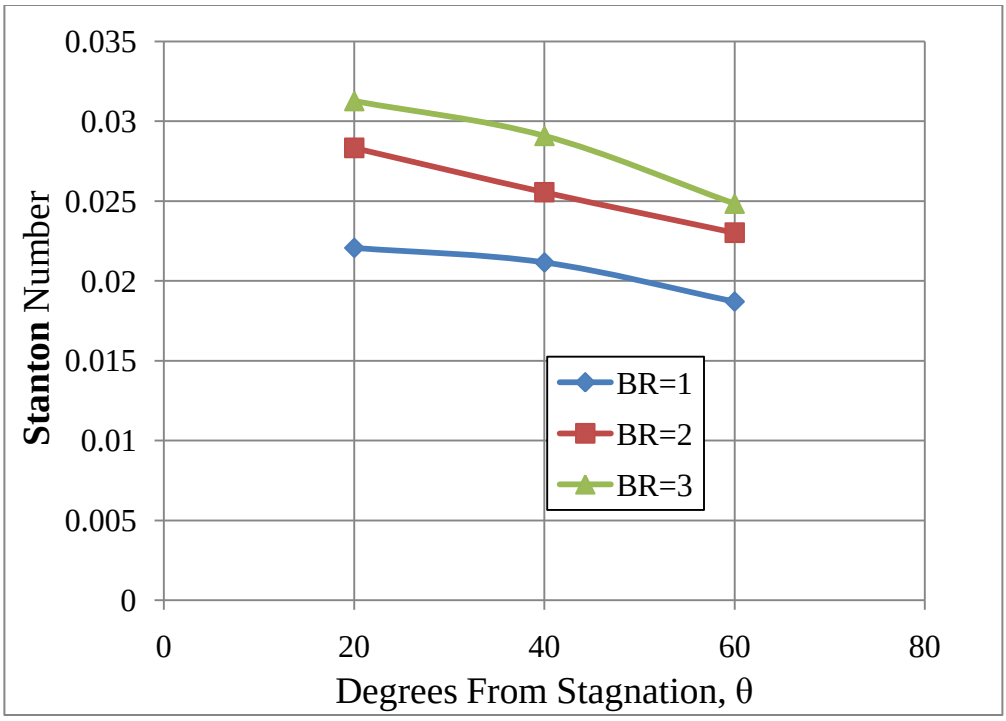

Figure 5.19. Convective heat transfer as function of angle for blowing ratios 1.0 - 3.0

5.5 Performance After Deposition

The semi-cylindrical surface was exposed to particle laden flow so the particle loading factor (PLF) would be equal to 100ppm-hr. This implies that each test case as outlined in Table 5.1 was exposed to the PVC particles for 12-15 minutes. After each run, the entire tunnel assembly was allowed to cool and the blade as removed from the test section. The semi-cylindrical surface was removed and a photo was taken. Then the PVC particles were scrapped off into a bag and the bag's total mass was measured on a scale. Care was taken to see that all particles were removed from the surface and the cooling holes were bored through. Then the detachable metal leading edge was scrubbed clean with alcohol and remounted on the blade body and reinstalled into the test section.

Figure 5.20 gives three sample photographs of the leading edge after deposition has occurred. All photographs are at a blowing ratio of 3.0 while T_1^* is 0.71, 0.8, and 0.9 from top to bottom. These images can be compared to the clean leading edge (deposit free) in Figure 5.10.

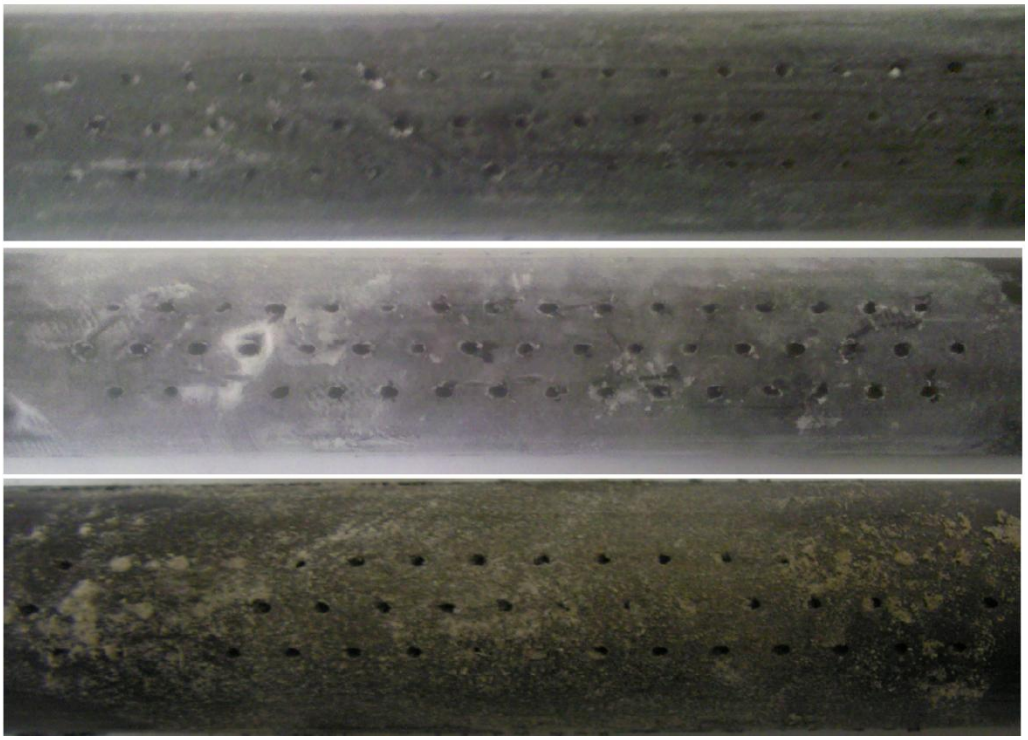

Figure 5.20. Photographs of leading edge with deposits for BR=3 at various temperatures

Results tabulating the capture efficiency are given in Table 5.3. It should be noted that it is assumed that all particles introduced into the flow approach the plate in this definition of capture efficiency Equation (2.6).

Table 5.3. Capture efficiency at several blowing ratios and temperatures on leading edge.

Blowing Ratio	**Free Stream Temperature, T_1^***	**%Capture Efficiency**
0	0.71	16.2
0	0.8	18.5
0	0.89	23.0
1	0.71	15.1
1	0.8	16.2
1	0.89	21.4
2	0.71	13.3
2	0.8	17.7
2	0.89	23.6
3	0.71	11.1
3	0.8	14.7
3	0.89	17.2

These results can be graphed, as shown in Figure 5.21.

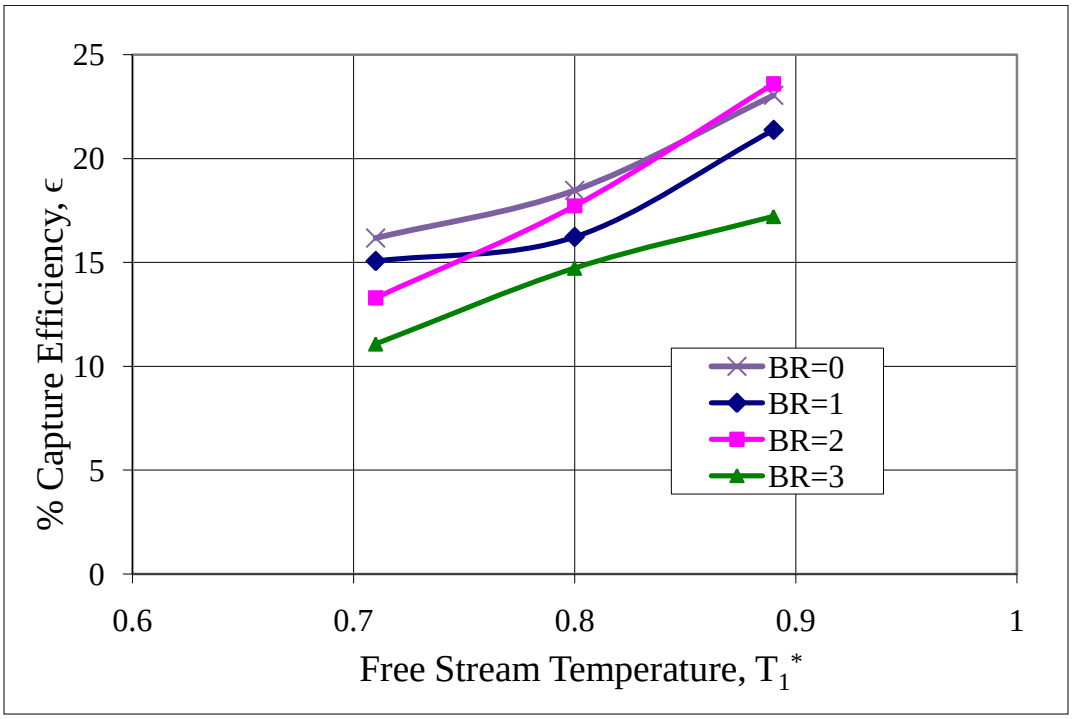

Figure 5.21. Graph of capture efficiency at various temperatures and blowing ratios.

There are two trends here to note. The first is that capture efficiency increases with free stream temperature. This is the same trend observed from the flat plate experiments. As the particles heat up, they become softer and less viscous which causes them to be more likely to stick to a surface. The second trend is that increasing the blowing ratio slightly decreases the capture efficiency. This trend is not as strong as the one with free stream temperature, but is still present. As the blowing ratio is increased the surface temperature drops. From the flat plate experiments, a lower surface temperature caused lower capture efficiency. Therefore, increasing the blowing ratio will decrease the amount of particles that deposit.

The numbers for capture efficiency presented in Table 5.3 are assuming every particle injected approaches the plate. This may not be accurate as many particles injected flow far away from the surface and never have a chance to impact. From observations after the experiments, it was seen that particles seem to be confined to a 2.5" diameter circle in the center of the flow field in the test section. Since the surface is only

5/8” thick, most of the particles flowing in the 2.5” circle do not approach the surface. Taking these area ratios into consideration, the capture efficiency can be recalculated with a smaller number in the denominator in Equation (2.6). These results are tabulated in Table 5.4. Note that these results are from the same experiments as Table 5.3, just with a different way of calculating capture efficiency.

Table 5.4. Capture efficiency results when projected area is taken into consideration.

Blowing Ratio	**Free Stream Temperature, T_1^***	**%Capture Efficiency**
0	0.71	42.1
0	0.8	48.1
0	0.89	59.8
1	0.71	39.3
1	0.8	42.1
1	0.89	55.6
2	0.71	34.6
2	0.8	46.0
2	0.89	61.4
3	0.71	28.9
3	0.8	38.2
3	0.89	44.7

An effort to determine the uncertainty in the capture efficiency was undertaken. The point at free stream temperature $T_1^* = 0.80$ and blowing ratio BR = 2.0 was repeated three more times. Four results from the same point had a standard deviation of 12% of its value. The same standard deviation can be applied to all points. For example, from Table 5.3, BR = 2.0, and $T_1^* = 0.80$; the range could be from 20.8% to 26.4%. The +/- one standard deviation error bars were not applied to Figure 5.21 because it would make it too confusing. It should be noted that with +/- one standard deviation causes several of the error bands to overlap. This indicates that the trend of decreased deposition with higher blowing ratio is a weak correlation.

In addition to measuring the amount of particles that have become deposited on the plate, an IR camera was used to measure changes in the film cooling effectiveness and convective heat transfer. This analysis was only done for the middle temperature

($T_1^* = 0.80$), but three blowing ratios. Figure 5.22 gives the raw IR images at blowing ratios of 1.0, 2.0, and 3.0 (top to bottom). Hot flow goes from the bottom to top of each individual image. Coolant flow foes right to left. Figure 5.23 gives the same data, but reduced into the contour plots that show effectiveness. Again, the blowing ratios are 1.0, 2.0, and 3.0 from top to bottom. Figure 5.13 can be used as a key to match color to effectiveness.

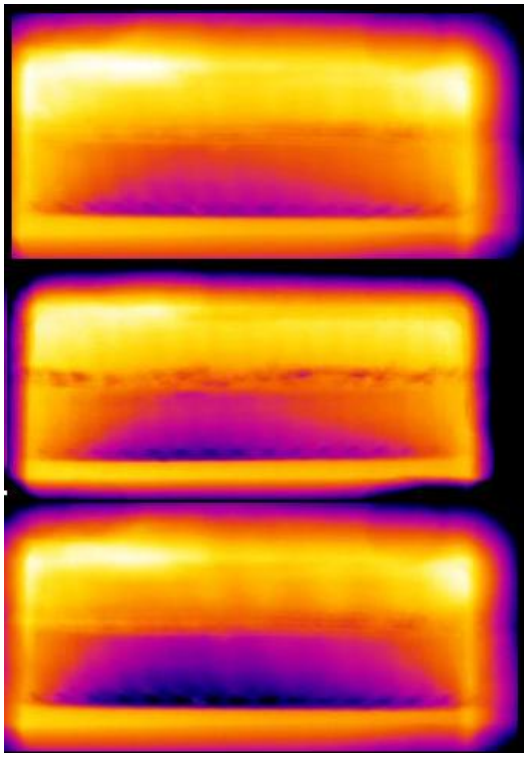

Figure 5.22. Raw IR images at various blowing ratios with deposits

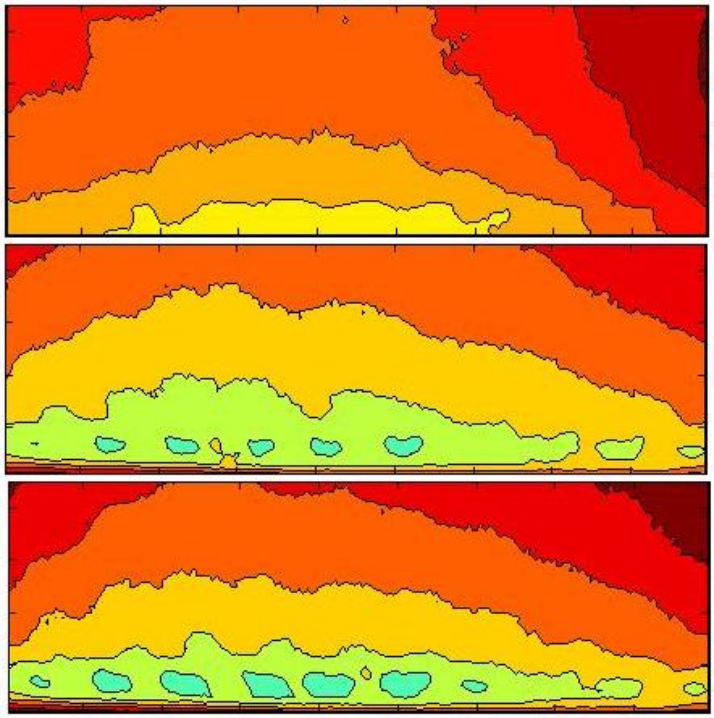

Figure 5.23. Contour plots of effectiveness with deposits

Figure 5.24, Figure 5.25, and Figure 5.26 show the film cooling effectiveness as a function of angle before and after deposition for blowing ratios of 1.0, 2.0, and 3.0 respectively. The general trend here is that deposits on the surface increase film cooling effectiveness. However, this may be in error due to the differences in emissivity as discussed in Chapter 3. PVC has a lower emissivity that gives a false lower temperature reading through the IR camera. A lower surface temperature reading translates to higher effectiveness. This error is thought to only be a few percent, but might be responsible for some of the augmentation in film cooling effectiveness presented here.

Positive augmentations to the film cooling effectiveness have been seen before in the literature by Sundaran and Thole [22] and by Lawson and Thole [23]. The increases in film cooling shown here are greater than those reported. This may be due to differences in geometry, particulate loading, and differences in non-dimensional temperatures, or by the error from emissivity as discussed above.

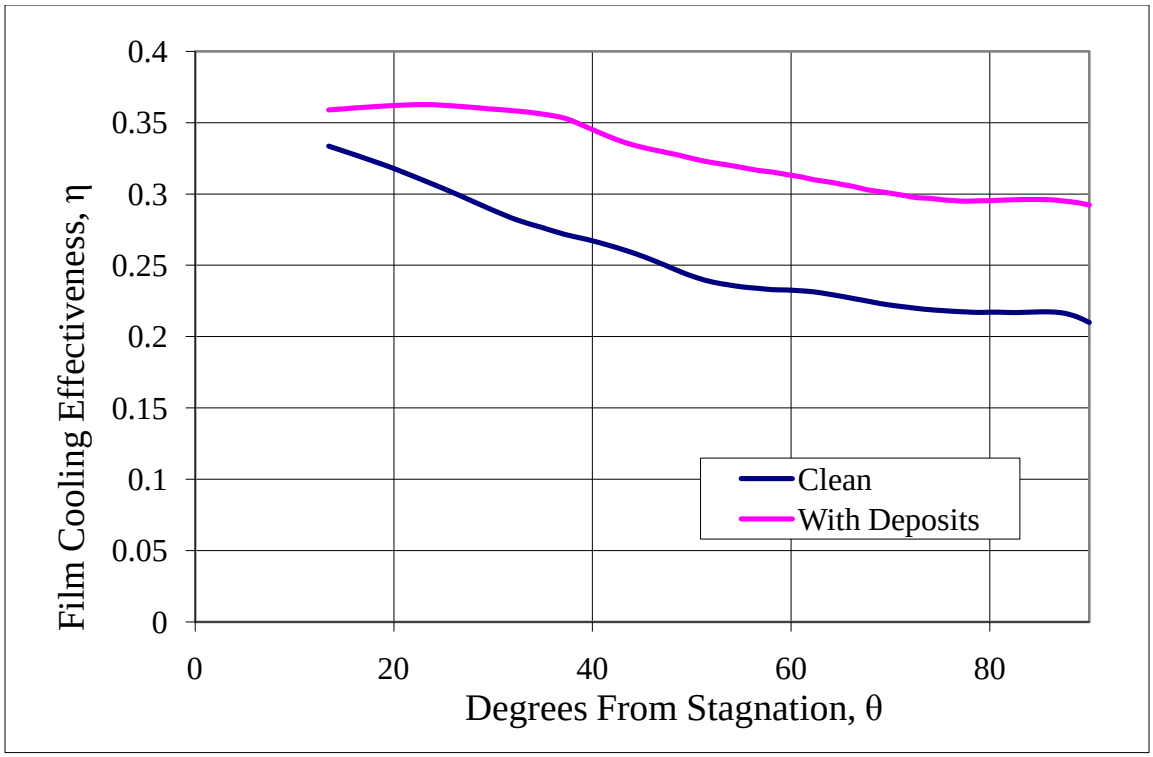

Figure 5.24. Change in film cooling effectiveness with deposits for BR = 1.0

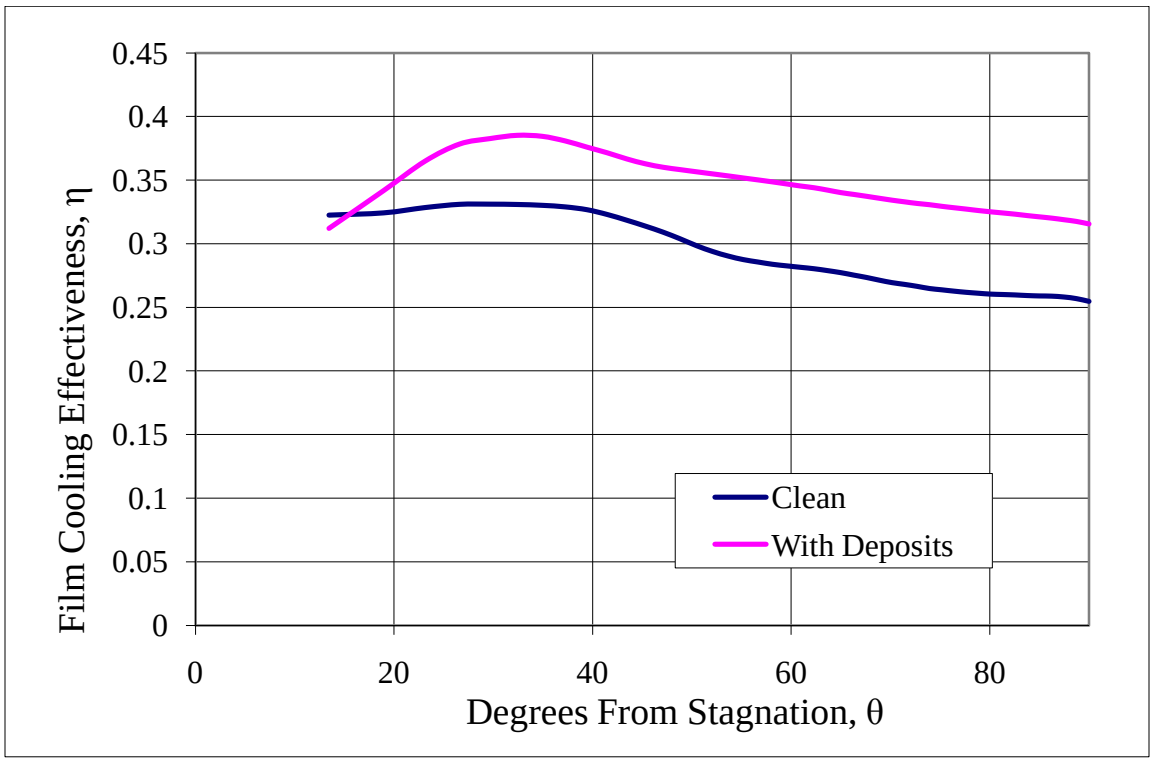

Figure 5.25. Change in film cooling effectiveness with deposits for BR = 2.0

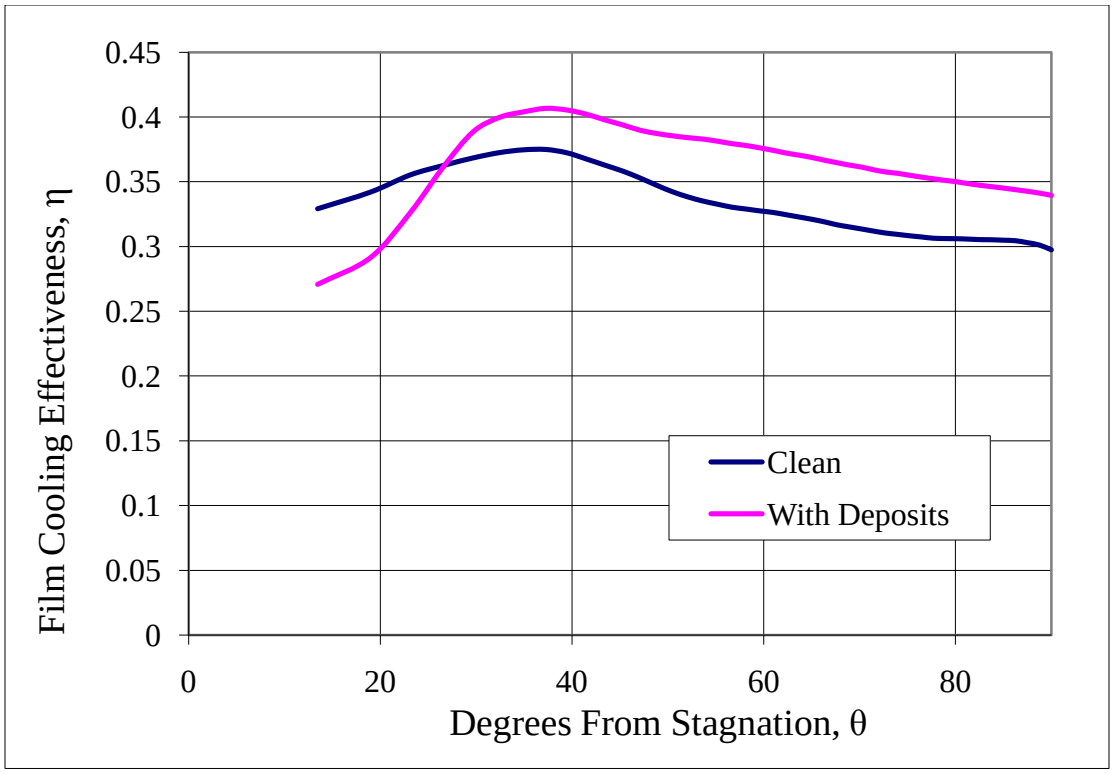

Figure 5.26. Change in film cooling effectiveness with deposits for BR = 3.0

The last effect deposition might have on the leading edge that is part of this study is changes on the convective heat transfer. The rough surface could cause extra turbulence near the surface resulting in a change in heat transfer between the air and the surface. Convective heat transfer has been made non-dimensional reported as the Stanton number. All of these tests were done at a free stream temperature of $T_1^* = 0.80$ and various blowing ratios. Figure 5.27, Figure 5.28, and Figure 5.29 give the augmentation of convective heat transfer as a function of angle before and after deposition has occurred. The general trend observed here is that deposits increase convective heat transfer, but not by much (20% at the most). These increases are similar to results by Bons [17] and Bogard et al. [19], but they saw greater increases in convective heat transfer (up to 50%). The difference in emissivity of PVC and black metal does not cause any error in these results because IR measured temperatures are only compared to itself. The h value only depends on the shape of the curve in Figure 3.9. Film cooling effectiveness measurements compare IR measured temperature to thermocouple measurements (Equation (3.3).

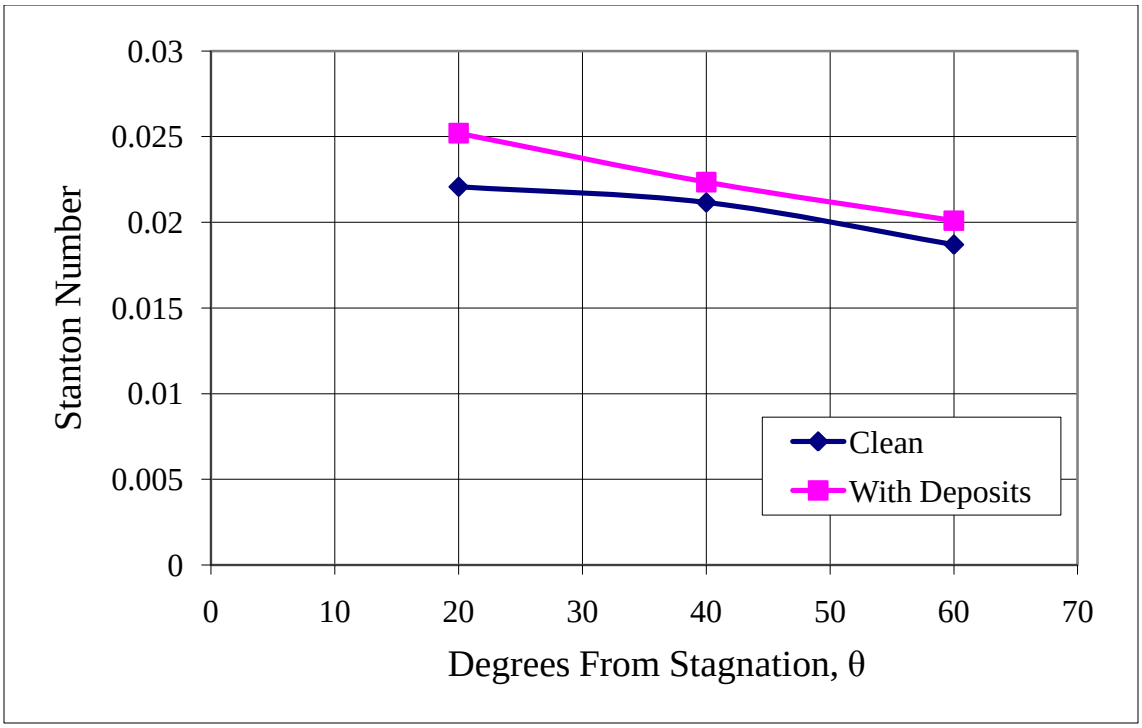

Figure 5.27. Augmentation to convective heat transfer by deposition at BR = 1.0

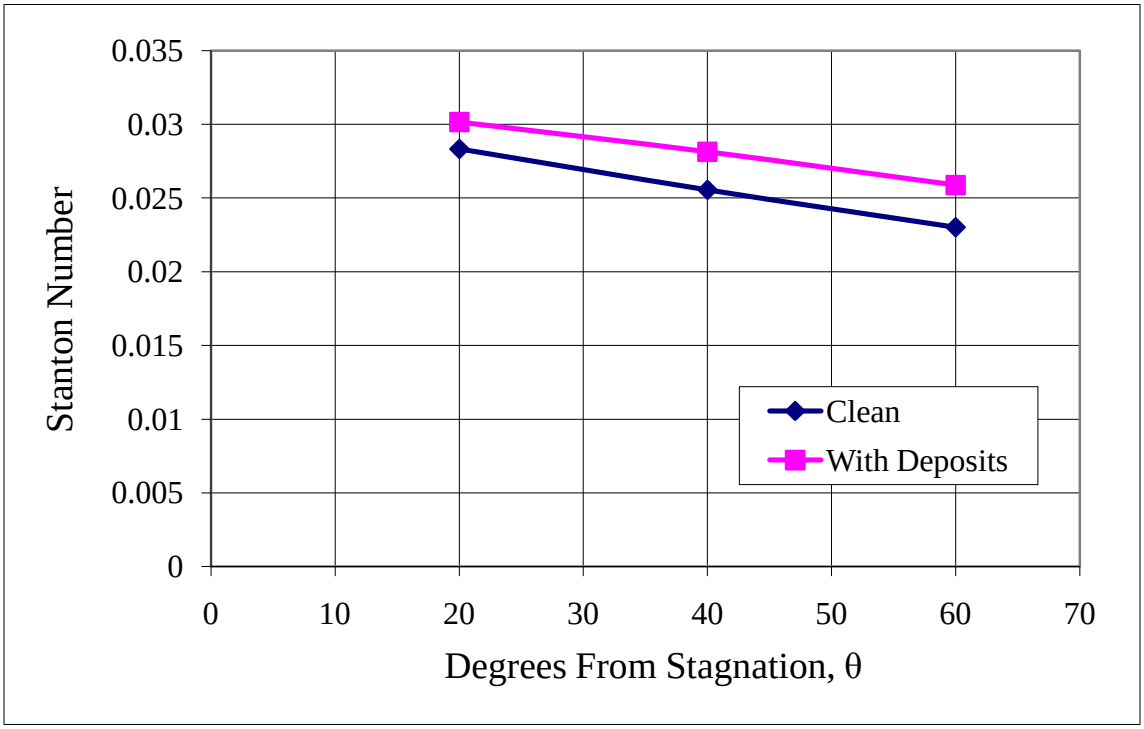

Figure 5.28. Augmentation to convective heat transfer by deposition at BR = 2.0

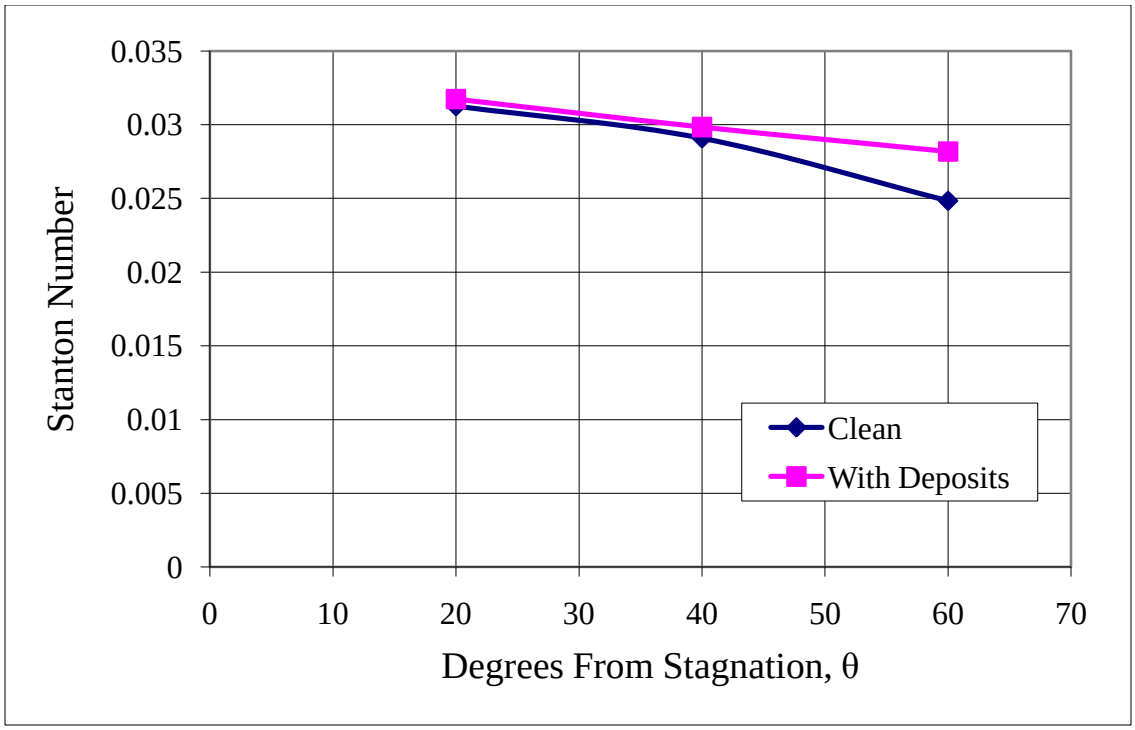

Figure 5.29. Augmentation to convective heat transfer by deposition at BR = 3.0

6 Conclusions

6.1 Review of Particle Substitution Method

A central component of this study is the use of the particle substitution method. Real gas turbines have a turbine inlet temperature in the 1500K range. This is a temperature above the range for most practical laboratory settings. It is common practice to do cascade testing of different air foil designs at room temperature. Heat transfer studies for different film cooling scheme can also be done at lower temperatures. It is desired to perform deposition studies at lower temperatures as well, but it is not as simple. A key indicator of whether or not a particle will deposit is how hot that particle is. Real coal ash particles deposit at temperatures near their melting point. Therefore, impacting coal ash at room temperature would not cause any deposition and experiments would fail.

A solution to this problem is to use some other particle that has a lower melting point. Therefore, the particles can still be at reasonably low temperatures and deposit on a surface. The method proposed in this study uses polymer particles, namely Teflon and PVC, to be used in place of coal ash. These materials still need to heated in order to reach near their melting point, but not nearly as much as coal ash. In the end, it was discovered that PVC works as a substitute material better than Teflon.

To scale experiments between substitute particles and real engine conditions, several non-dimensional quantities have been proposed. Fist, a ratio of the free stream temperature to the melting point of the particle has been defined. This sets the free stream temperature during experiments to a more reasonable level. This non-dimensional temperature has been labeled T_1^* (Equation (2.2). The next non-dimensional temperature factors in the surface temperature, since that is known to influence deposition. T_2^* has been defined as the ratio of the difference in melting temperature of the particle and the free stream to the difference of the melting and surface temperatures (Equation (2.3).

The first two parameters set the free stream and the surface temperatures. The next variable in the flow condition to set is the free stream velocity. This is done by matching

the particle momentum stokes number (Equation (2.4). Differences in the particle's size and density are taken into account and the velocity is set as to keep the Stokes number between the engine conditions and experiment as close as possible. Since the PVC particles are larger than coal ash, this experiment was done at a lower velocity than one might find in an engine.

The last part of the particle substitution method is to set the particle loading factor. The PLF (Equation (2.5) is used to speed up the experiment. For deposition in syngas fueled turbine to cause problems, it needs to accumulate over thousands of hours of operation. This is also not practical for a laboratory setting. For experiments, the particle concentration in the hot flow is greatly increased and the time is greatly reduced. A real turbine at a particle concentration of 0.02ppm firing for 5000 hours can be equivalent to an experiment with a particle concentration 0f 400ppm running for 15 minutes (1/4 hour). Both have a PLF of 100ppm-hr.

6.2 Summary of Results

The experiments presented in this study come in two parts. The first is a validation on the particle substitution method outlined above. The second part uses the method with a more complex geometry and with film cooling.

The validation experiment deposited both Teflon and PVC on a flat plate. The whole experiment was set up to mimic a published study by Crosby et al. [14], who used real coal ash particles at engine like conditions. This experiment consisted of two series. The first varied only the free stream temperature and observed the effect on deposition amount. The other series cooled the surface and measured the effect on deposition. The first trend here was that increasing the free stream temperature increases the deposition. The other trend was that decreasing the surface temperature decreased the deposition amount. Both of these trends were observed for all materials.

Although the trends matched up, the results for all materials were not the same. PVC tended to have more deposition than coal ash, which tended to have more deposition than the Teflon. The discrepancies can be attributed to material properties not well understood that were not considered in this study. Because the results were similar, it

was decided that using polymer particles as a substituted material can successfully be used. It was also found that PVC had a stronger temperature correlation and was easier to handle.

The second half of this study used PVC and the particle substitution method to study deposition on a leading edge of a blade or vane. For this experiment, a high temperature low turbulence wind tunnel was constructed. The test section was rectangular and the deposition target was a semi-cylindrical leading edge with a flat after body. The leading edge had 49 cooling holes to allow for film cooling.

The leading edge was characterized to find the adiabatic film cooling effectiveness and convective heat transfer coefficient before deposition took place. A plastic model was also used to get the true adiabatic film cooling effectiveness. The trends observed here were that higher blowing ratios both increased the film cooling effectiveness and increased the convective heat transfer.

The leading edge was exposed to PVC particle laden flows and then the heat transfer and cooling effectiveness were reexamined. It was found that surface deposition on the leading edge generally had higher film cooling effectiveness. It was also found that the deposition slightly increased the convective heat transfer into the blade. This is most likely due to the extra surface roughness causing more turbulence near the leading edge. The amount of film cooling and heat transfer testing was limited due to limited access to the IR camera.

The capture efficiency was also measured on this geometry as a function of both blowing ratio and free stream temperature. Non-dimensional free stream temperature (T_1^*) was varied from 0.71 to 0.89 and blowing ratio was varied from 0 (no cooling) to 3.0. It was found that increasing the free stream temperature increased the amount of deposition. Additionally, increasing the blowing ratio (and thereby lowering the surface temperature) caused there to be slightly less deposition. Both of these trends are similar to the results from the flat plate testing.

6.3 Suggestions for Further Investigations

The research topic of syngas ash deposition is relatively new and many aspects are still not known. There is ample future work to be done in this field that could be completed using the methods described in this study.

All free stream temperatures in this study were below the melting point of the particulate material ($T_1^* < 1$). Since both the melting point of coal ash and the turbine inlet temperature of engines both vary greatly, it is entirely possible that particles will be above the melting point when they impact on a surface. If the particles were to undergo a phase change and become molten while still in the air, there might be substantial differences in the deposition amount. Also, if the surface temperature is above the melting point of the particulate material, the particles may never solidify and become deposited. Further experiments with varying the temperatures above melting would be useful to advance knowledge in this area.

Another possible study in the topic of ash deposition would be to vary the shape of the cooling holes. The cooling holes in this study were straight cylinders. It is believed that using trenched cooling holes provide better film cooling performance. A study of syngas ash deposition on a leading edge that has holes of more complex shapes could provide more solutions to the deposition problem.

A final recommendation for a future study would be to measure how the discharge coefficient changes as deposition builds up. As particles accumulate around cooling holes, constrictions, burrs, and elongation could occur. This would change how much coolant passes out of the holes and through the inner channels.

7 References

1. Bons, J.P., Crosby, J.M., Wammack, J.E., Bentley, B.I., Fletcher, T.H., 2005, "High Pressure Turbine Deposition in Land Based Gas Turbines from Various Synfuels," GT2005-68479.

2. Borom, M. P., Johnson, C. A., and Peluso, L. A., 1996, "Role of Environmental Deposits and Operating Surface Temperature in Spallation of Air Plasma Sprayed Thermal Barrier Coatings," Surface and Coatings Technology 86-87, pp. 116-126.

3. Seggiani M., Pannocchia G., 2003. "Prediction of Coal Ash Thermal Properties Using Partial Least Squares Regression". Ind. Eng. Chem. Res., Vol. 42, No. 20, pp 4919-4926.

4. Hamed, A., 1988. "Effect of Particle Characteristics on Trajectories and Blade Impact Patterns". Journal of Fluid Engineering, Vol. 110, pp 33-37.

5. Smialek, J.L., Archer, F.A., Garlick, R.G., 1992. "The Chemistry of Saudi Arabian Sand: a Deposition problem on Helicopter Turbine Airfoils". 3rd International SAMPE Metals and Metals Processing Conference, Society for the Advancement of Material and Process Engineering, Vol. 3, pp M63-M77.

6. Kim, J., Dunn, M.G., and Baran, A.J., 1993, "Deposition of Volacanic Materials in the Hot Sections of Two Gas Turbine Engines," J. Engr. Gas Turbines & Power vol. 115, Jul 1993, pp641-651.

7. Hamed, A., Tabakoff, W., Wenglarz, R., 2006, "Erosion and Deposition in Turbomachinery," *J. Propulsion and Power*, **122 (**2), pp. 350-360.

8. Dring, R. P., Casper, J. R., and Suo, M., "Particle Trajectories in Turbine Cascades," *Journal of Energy*, 1979, Vol. 3, No. 3, pp. 161–166.

9. Wenglarz, R.A., and Wright, I.G., 2003, “Alternate Fuels for Land-Based Turbines,” *Proceedings of the Workshop on Materials and Practices to Improve Resistance to Fuel Derived Environmental Damage in Land-and Sea-Based Turbines,* Oct. 22-24, Co. School of Mines, Golden, Co., pp. 4-45 to 4-64.

10. Tabakoff, W., Hamed, A., and Wenglarz, R., 1988, *Particulate Flows and Blade Erosion*, Lecture Series Publ., von K´arm´an Inst. for Fluid Dynamics, Rhode-Saint-Genese, Belgium, No. 2, , pp. 34–40.

11. Wenglarz, R.A., and Fox, R.G., 1990, “Physical Aspects of Deposition from Coal-Water Fuels Under Gas Turbine Conditions,” J. of Engineering for Gas Turbines and Power, **112**, pp. 9-14.

12. Logan, R.G., Richards, G. A., Meyer, C. T., Anderson, R. J., 1990, “A Study of techniques for Reducing Ash Deposition in Coal-Fired Gas Turbine,” Progress in Energy and Combustion Science. Vol. 16, pp. 221 – 223.

13. Ahluwalia, R. K. , K. H. Im, and R. A. Wenglarz, "Flyasb Adhesion i n Simulated Coal-Fired Gas Turbine Environment," ASME Paper GT-135 Presented a the Gas Turbine and Aeroengine Congress and Exposition, Amsterdam, The Netherlands, June 5-9, 1988.

14. Crosby, J.M., Lewis, S., Bons, J.P., Ai, W., Fletcher, T.H., “Effects of Particle Size, Gas Temperature, and Metal Temperature on High Pressure Turbine Deposition in Land Based Gas Turbines from Various Synfuels”, 2007, GT-2007-27531.

15. Bons, J.P., Taylor, R., McClain, S., and Rivir, R.B., 2001, “The Many Faces of Turbine Surface Roughness,” ASME J. Turbomach., 123, No. 4, October 2001, pp. 739 - 748.

16. Wenglarz, R. A., “An Assessment of Deposition in PFBC Power Plant Gas Turbines,” *Journal of Engineering for Power,* Vol. 103, No. 3, 1981, pp. 552–560.

17. Bons, J. P., 2002, ‘‘St and cf Augmentation for Real Turbine Roughness with Elevated Freestream Turbulence,’’ ASME J. Turbomachinery., **124**, pp. 632–644.

18. Bons, J.P., Wammack, J.E., Crosby, J., Fletcher, D., and Fletcher, T.H., 2006, “Evolution of Surface Deposits on a High Pressure Turbine Blade, Part II: Convective Heat Transfer,” GT-2006-91257.

19. Bogard, D.G., Schmidt, D.L., Tabbita, M., “Characterization and Laboratory Simulation of Turbine Airfoil Surface Roughness and Associated Heat Transfer,” J. Turbomachinery. Vol 120, April 1998, pp 337-342.

20. Schmidt, D.L., Sen, B., Bogard, D.G., 1996. “Effects of Surface Roughness on Film Cooling,” ASME Paper No. 96-GT-299.

21. Lewis, S., Barker, B., Bons, J. P., Weigou, A., and Fletcher, T. H. 2009. “Film Cooling Effectiveness and Heat Transfer Near Deposit-Laden Film Holes.” GT2009-59567.

22. Sundaram, N., Thole, K., “Effects of Surface Deposition, Hole Blockage, and Thermal Barrier Coating Spalation on Vane Endwall Film Cooling,” J. Turbomachinery. Vol 129, July 2007, pp 599-607.

23. Lawson, S.A., Thole, K., “The Effects of Simulated Particle Deposition on Film Cooling,” presented at ASME Turbo Expo: Power for Land, Sea, and Air. June 8-12, 2009, Orlando, Florida USA. Paper #: GT2009-59109.

24. Ai, W., Murray, N., Fletcher, T. H., Harding, S., Bons, J. P. 2009. “Effect of Hole Spacing on Deposition of Fine Coal Fly Ash Near Film Cooling Holes.” GT2009-59569.

25. Kuo, Y.M., Wang, J.W., Wang, C.T., Tsai, C.H, 2007, "Effect of Water Quenching and SiO2 Addition During Vitrification of Fly Ash". Department of Safety Health and Environmental Engineering, Chung Hwa University of Medical Technology, Tainan County, Taiwan.

26. Jensen, J.W., Squire, S.W., Bons, J.P., Fletcher, T.H., 2005, "Simulated Land Based Turbine Deposits Generated in an Accelerated Deposition Facility" *J. of Turbomachinery,* **127**, pp. 462-470.

27. Sreedharan, S. S., and Tafti, D., 2010. "Composition Dependent Model for the Prediction of Syngas Ash Deposition with Application to a Leading Edge Turbine Vane", GT2010-23655.

28. Cutbirth, J. M., and Bogard, D. G., 2003, "Effects of Coolant Density Ratio on Film Cooling Performance on a Vane," ASME Paper # GT2003-38582.

29. Abuaf, N., Bunker, R., Lee, C. P., 1997, "Heat Transfer and Film Cooling Effectiveness in a Linear Airfoil Cascade," *Journal of Tubomachinery,* vol. 119, pp. 302-309.

30. Mehta, R.D. and Bradshaw, P., 1979, Design rules for small low speed wind tunnels," Aeronautical Journal, November 1979, p443-449.

31. ASME Pressure Vessel and Boiler Code Section VIII Appendix 13, 2006, Pressure Vessels of Non-Circular Cross Sections.

Appendix

Matlab program used for data reduction with IR camera used to find effectiveness

```
%%Used for finding cooling effectiveness for curved blade
%%Assume IS camera is 20 deg off vertical
%%Input important stuff here
Raw = DEPS1;  %Inport data first, name
pt1 = [225, 454];
pt2 = [393, 408];
Tinf = 434; %degrees K
Tcool = 350;
E = 1;  %emissivity
Tamb = 292;
Ucool = 25;  %jet coolant velocity m/s
Mcool = Ucool * (2.43e-5) / (1.2 * 300 / Tcool);
Qdp = Mcool * 1005 * (Tcool - Tamb) / (0.037);  %W/m2
DTcorr = Qdp * 0.00254 / 16;

%%Extract Blade data
RawT = Raw' / E + DTcorr;
Blade = RawT([pt1(1):pt2(1)], [pt2(2):pt1(2)]);
Blade = flipdim(Blade', 1);
%%contourf(Blade')

%%Weight Factor
S = size(Blade);
R = S(1);
WF = zeros(R, 1);
   for i = 1:R
        WF(i, 1) = (i-1)/R;
   end

WF = acos(1 - WF - 0.35); %%0.35 corresponds to camera angle (radians)
WF = 1 ./ sin(WF);

%%Area Weighted Average
T = zeros(R, 1);
for i = 1:R
    T(i, 1) = mean(Blade(i,:));
end

Tavg = T .* WF;
Tavg = sum(sum(Tavg)) / sum(sum(WF))
n_global = (Tinf - (Tavg + 273)) / (Tinf - Tcool)

%Plot n as function of angle
theta = zeros(R, 1);
space = zeros(R, 1);
for i = 1:R
    space(i, 1) = WF(i, 1) / (sum(sum(WF)));
end
for i = 2:R
```

```
    theta(i, 1) = theta(i-1, 1) + space(i-1, 1);
end

theta = acos(1 - theta);

n_local = (Tinf - (T + 273.15)) / (Tinf - Tcool);

%Contour plot setup

c = [0; 0.025; 0.05; 0.075; 0.1; 0.125; 0.15; 0.175; 0.2;
    0.225; 0.25; 0.275; 0.3; 0.325; 0.35; 0.375; 0.4; 0.425; 1];

map = (Tinf - (Blade + 273.15) ) / (Tinf - Tcool);

subplot(2,1,1); contourf(Blade, c)
subplot(2,1,2); plot(theta, n_local)
```